NTNU – Trondheim
Norwegian University of
Science and Technology

A Comparison of Biological Dose Estimates in Proton and Carbon Ion Therapy Based on Averaged and Full Linear Energy Transfer Spectra

Eivind Rørvik

Master of Science in Physics and Mathematics
Submission date: July 2015
Supervisor: Pål Erik Goa, IFY

Norwegian University of Science and Technology
Department of Physics

Abstract

Radiotherapy with ions, also known as particle therapy, is increasing rapidly. Shifting from photons to protons and carbons is not only a great technological transition, but also a shift in physics and in radiobiology. To adapt from the higher biological effectiveness of particles compared to photons, the concept of relative biological effectiveness (RBE) is used. Protons are slightly more effective than photons, and the RBE is set to be constant 1.1. The constant RBE value is not a physical property of the beam, it is simply assigned to be 1.1 by a consensus in the scientific community. Experiments indicate that the RBE in reality is marginally increasing along with the treatment depth. For carbon ions the variations in RBE are significantly higher and typically range between 1 and 3. The variation is taken into account in treatment planning, however, relatively large uncertainties are present in the radiobiological models applied. Many of these models are based on correlations between the calculated linear energy transfer (LET) and experimentally measured RBE. Most phenomenological models are based on the dose averaged LET, LET_d. However, it should also be possible to correlate the biological effect to the full dose weighted LET spectrum, $d(L)$. By using a biological weighting function (BWF), it is possible to estimate the RBE from either LET_d or $d(L)$.

In this work, several proton and carbon ion beams were simulated with the FLUKA Monte Carlo code. The physical absorbed dose and the LET spectrum $d(L)$ were estimated at different depths in a water phantom. A BWF was created upon existing cell experiments databases and applied to quantify the effect of the averaging. The biological effective dose (BED) was then estimated on either the average or the full LET spectrum.

The difference between the calculated BED of the two methods are under 2% for protons, as long as the BWF is close to linear in the relevant LET range. If the BWF is non-linear in the low LET region, the two estimates differ up to 17 %, specially in the distal part of the spread out Bragg Peak (SOBP) and the in the distal dose falloff. However, for carbon ions, the dose estimates are significantly different. In particular, this is observed along the SOBP, where the

BED estimated by the spectrum method is approximately 15% under the BED of the average method.

The results show that calculating the RBE by the averaging the dose weighted LET spectrum has little impact on the estimated BED from protons, as long as a linear approximation of the LET-RBE relation is chosen. The two estimates differs considerably for carbon ions, due to the peak in relevant LET region of the BWF. This difference should not be neglected, ergo it is not recommended to average the LET spectrum in radiobiological models used for carbon ion therapy. The implementation of the LET spectrum method could also be adapted to other radiobiological models based upon LET_d.

Samandrag

Stråleterapi med ion, også kjend som partikkelterapi, veks snøgt. Men å gå ifrå behandling med foton til proton og karbon ion inneber ikkje berre ei stort teknisk skifte, men og ei skifte i den bakenforliggande fysikken og strålebiologien. For å tilpasse seg den høgare biologiske effekten av partiklar sammenligna med foton, er begrepet relativ biologisk effektivitet (RBE) innført. Proton er berre litt meir effektive enn fotoner, så RBE verdien er satt til å vere konstant 1,1. Den konstante RBE verdien er ikkje ein fysisk eigenskap av strålen, den er bare satt til å vere det av ein konsensus i det vitenskapelege miljøet. Men i realiteten tyder eksperiment på at RBE stig marginalt med behandlingsdybda. For karbon ion er variasjonen i RBE er vesentleg høgare og typisk i området mellom 1 og 3.

Variasjonen tek ein hensyn til i behandlingsplanlegginga, sjølv om det er relativt store usikkerheiter i RBE, avhengig av den strålebiologisk modellen som blir brukt. Mange av desse modellane er basert på sammenhengar mellom den beregna *linear energy transfer* (LET) og eksperimentelt målte RBE. Dei fleste fenomenologiske modellane er basert på det dosevekta LET snittet, LET_d. Men det bør og vere mogleg å koble RBE opp mot den biologiske effekten til full det dosevekta LET-spektret, $d(L)$. Ved å bruke ein biologisk vektingsfunksjon (BWF), er det mogleg å anslå RBE fra enten LET_d eller $d(L)$.

I dette arbeidet blei fleire proton- og karbonionestråler simulert med FLUKA Monte Carlo kode. Den fysiske absorberte dosa og LET spekteret $d(L)$ blei funne på forskjellege dybder i eit vannfantom. Ein BWF ble laga med data frå eksisterande celleforsøk og brukt for å kvantifisere effekten av gjennomsnittinga. Den biologiske effektive dosa (BED) blei så beregna på enten med den snittverdien av LET spekteret eller det fulle LET spekteret.

Forskjellen mellom den beregna BED av dei to metodane er under 2% for proton, enn så lenge BWF er tilnærma lineær i det aktuelle LET området. Dersom BWF er ikkje-lineær i den låge LET-regionen, kan dei to anslaga variere opp til 17%, spesielt i enden av *spread out Bragg peak* (SOBP) og langs det distale dosefallet. Men for karbonion, er estimatene er vesentleg forskjellege. Forskjellen er spesielt stor langs SOBPen, der BED er estimert med spekter metoden er

tilnærma 15% under BED av den gjennomsnittlege metoden.

Resultata viser at beregning av RBE av gjennomsnittleg dosevekta LET spekter har lita innvirkning på den estimerte BED fra proton, enn så lenge ei lineær tilnærming av LET-RBE forhaldet ligg til grunn. Men anslaga avviker betydeleg for karbon ioner, på grunn av maximumet i BWF. Denne forskjellen bør ikkje neglisjerast, med andre ord: Det er ikkje anbefala å bruke gjennomsnitt LET spektrum i strålebiologiske modellar som brukas for stråleterapi med karbon ion. Gjennomføringa av LET spekter metoden kan og tilpassas andre strålebiologiske modeller basera på LET_d.

Acknowledgements

I would like to thank everyone who have supported me during the work with this thesis. Since I started to look for the possibility to write a thesis on particle therapy, I've only met good will from all parts. It has been a highly motivating process.

First I would like to thank my supervisor, Pål Erik Goa, whom "hijacked" me and gave me the opportunity to write a master thesis on particle therapy thesis at my own home university. I have enjoyed the advices, the professional discussions and the relaxed atmosphere.

I appreciated the interest shown from the medical physicists at the radiotherapy clinic of St. Olav University Hospital. Especially Sigrun Saur Almberg, whom unmotivated asked for proofreading my thesis, which turned out to be quite some work.

I would also like to thank Odd Harald Odland of Haukeland University Hospital and Dieter Röhrich of University of Bergen, whom openly replied to my request on writing a thesis. I'm grateful for the cooperation with the group.

From this group, I would specially thank Kristian Smeland Ytre-Hauge. He has done far more than could be expected from a non-affiliated supervisor. I am most grateful for the weekly hour long phone conversations, late night mail correspondence and eager proofreading. I glad for the technical discussions, the criticism and the support given. The same relevant competence and open helpfulness are not found any other place in Norway. I appreciated the Monte Carlo Workshop last fall and the week this spring I was able to stay at the University of Bergen. I also especially want to talk for the funding and companionship to the 3. ESTRO Forum.

I really glad the John Alfred Brennsæter joined me on writing a thesis on particle therapy. Thanks for the help in finding interesting articles. And even more interesting YouTube-clips.

I would also thank my other classmates, and especially Daniel Wennberg. I would have failed half of the lab courses without you. And for the opportunity to steal your idea and win an iPad.

I'm grateful for the everlasting support from my parents. Thanks for having me, I promise I have behaved. And to my brothers Tor Jakob, Jon Vegard and Asbjørn: Thanks for the inspiration! I don't think you know the sound of "NTH-ringen" as it strucks "vernepliktsmedaljen" yet, but you going to hear it every Christmas from now on.

And to Ruth, you were a pleasant distraction to the writing of the thesis.

Contents

Chapter 1

Introduction

Radiotherapy is one of the three main modalities used for cancer treatment. Around 52 % of all cancer patients in Norway receive radiotherapy as part of their treatment [1]. Technological developments in external radiotherapy have opened up new capabilities to treat difficult sites with higher precision and conformity. The introduction of Intensity Modulated Radiation Therapy (IMRT) in the 1990s and Volumetric Modulated Arc Therapy (VMAT) in the 2000s made better optimizations of the treatment fields to the shape of the tumour. However, the steadily increase in dose conformity driven by technology might be about to converge towards a physical limit, as illustrated in figure 1.1. This is due to the spatial dose distribution resulting from of photons and electrons [2, 3].

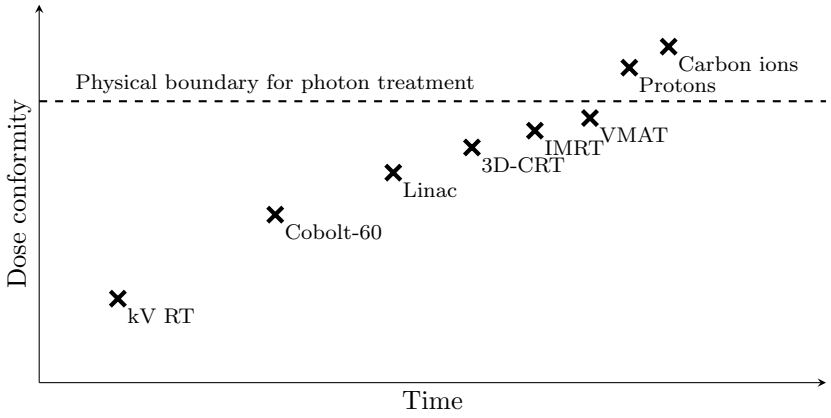

Figure 1.1: A qualitative overview over the major developments in external radiation therapy. The figure is only made for illustration purpose, and the positions in both directions are highly general arbitary and general.

Dose conformity is of special importance in cases where organs at risk (OAR) are close to the tumour [4]. Treatment with photons can result in a high normal tissue complication probability (NTCP), which in some cases is medically unacceptable. Better dose conformity can be achieved by treating with ions instead of photons. The ionization curve of ions, the Bragg curve, is more optimal for tumour coverage than the depth dose distribution of photons. According to a recent report [5], 10-15% of all cancer patient receiving radiotherapy are likely to benefit from treatment with protons and carbon ions. In Norway alone, this accounts for around 1500 people every year.

All of the new developments within conventional photon therapy, from 3D-RT to VMAT, are incremental innovations in the field. The same physics and radiation biology still hold for every technological step. However, by changing from conventional therapy with photons to particle therapy with ions, the radiation science also changes. The radiation quality is higher, meaning that ions are more effective in the inactivation processes of living cancer cells. If the same amount of physical dose, the energy deposited per unit mass, is given with conventional and particle therapy, the latter will kill more cells. This difference is not negligible, and must be accounted for in particle therapy. The variations in biological effect for the same physical dose is reflected by the relative biological effectiveness (RBE), a scaling factor.

Protons have only a slightly elevated RBE compared to photons. Based upon experiments with animal systems in the 1970s, the RBE for protons was set to be 1.1 [6]. This parameter was defined to be constant and independent of dose/fraction, tissue type and the beam characteristics. Today, 1.1 is still the value used in clinics, even though it is observed that the RBE increases along the treatment depth, as indicated in figure 1.2. For carbon ions, the issue of a variable RBE is even more present; the RBE typically varies from 1 at the entrance to 3 at the Bragg Peak [7] [8].

Good modelling of the RBE is needed to predict the biological effective dose (BED). Many different models have been developed over the last decades [9]. Some of the models are purely phenomenological; they simply measure a correlation between the physical and biological quantities and the RBE. The quantities include everything from cell type and particle type to radiation quality. Radiation

quality could be defined by the *linear energy transfer* (LET) of the radiation. LET is a non-stochastic quantity dependent on the energy of the particle. In a clinical setting, multiple types of particles with different energies traverses the medium. The radiation quality could then be described by a spectrum of different LET values at every spatial location. The standard procedure is to find the dose average LET value, LET_d, which is then used as an input parameter in the radiobiological model [10]. But the process of averaging might induce increased uncertainty in the RBE estimates, as some information about the radiation quality of the beam is lost [11].

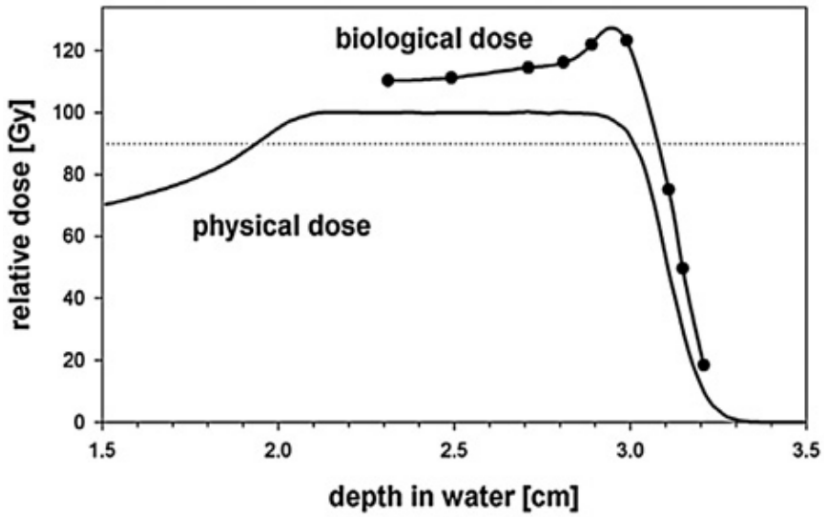

Figure 1.2: An example of a physical depth dose distribution for a proton spread out Bragg peak (SOBP). The biological effective dose (BED) is plotted above the physical dose, indicating the higher effectiveness for protons over photons. As seen, the BED increases at greater depths, and the RBE is therefore not constant in this model [12].

In this thesis, the effect of averaging the LET vs. keeping the full spectrum as input parameter for a phenomenological radiobiological model was investigated, and the resulting BEDs were compared. This was done by estimating the dose distribution and LET spectra from Monte Carlo simulations of clinical realistic proton and carbon ion beams. The RBE and BED at different depths was found by the use of a biological weighting function (BWF), developed from cell experiments found in two databases [13, 14].

Chapter 2

The physics of particle therapy

2.1 Stopping power

More than 100 years ago William Henry Bragg observed how alpha particles deposited their energy in different target material. He described the retarding force inflicted by the matter on the particles [15] [16]. This force is mainly due to elastic scattering with atomic electrons and the energy loss from this process is referred to as the stopping power. When the particle traverses through the material, atoms are ionized by the fast particle and "steals" some of its energy. Delta electrons are created, which further ionize the atoms locally in the wake of the ion.

Niels Bohr introduced in 1913 a theoretical model for the stopping power, and defined the stopping power to be the "linear rate of energy loss per unit path length":

$$S = -\frac{dE}{dl}. \tag{2.1}$$

The most common units for S is KeV/μm or MeV/nm. Bohr deduced his model upon classical physics, and the model was a bit low compared to experimental values.[17]

In 1930, Hans Bethe analytically deduced a new model for stopping power based upon quantum mechanics [18]. After some corrections and including relativistic effects, the model for stopping power could be written as: :

$$S = -\frac{\mathrm{d}E}{\mathrm{d}l} = \frac{4\pi}{m_e c^2}\frac{nz^2}{\beta^2}\left(\frac{e^2}{4\pi\epsilon_0}\right)^2\left(\frac{1}{2}\ln\frac{2m_e c^2\beta^2\gamma^2 T_{max}}{I^2} - \beta^2 - \frac{\delta(\beta\gamma)}{2}\right) \tag{2.2}$$

where m_e is the electron mass, c the speed of light, n the electron density of the

material, z is the charge of the particle, β is the momentum of the particle, e is the elementary electric charge, ϵ_0 is the permittivity of vacuum, T_{max} is maximum energy transfer of the particle, I is the mean excitation potential and $\delta(\beta\gamma)$ is a density correction. The stopping power is therefore dependent of the charge, mass and energy of the ion.

2.2 Coulomb scattering

When ions come close to the nuclei of the target material, the ions receive an angular shift in the trajectory due to Coulomb scattering. The angular shift will then have a gaussian statistical distribution, with the mean at 0 degrees [19]. The sigma of the distribution is then dependent on the material which the ions are passing through. Material consisting of light nuclei with low Z, like hydrogen or carbon, will give a low sigma, while high Z, like lead, will give a high sigma.

Another important difference between ion beams and electron beams is the level of scattering. Since ions are much heavier compared to electrons, they also scatter less in every interaction. This means that the penumbra is much smaller, giving a higher lateral precision for proton beams. In the same way, heavy ions like carbon ions will scatter less than lighter ions, as protons [19].

2.3 Nuclear interactions

The probability of inelastic interactions with nuclei is far lower than for interactions with electrons and elastic scattering. However, these reactions are still of significance for radiation therapy. The accelerated ions are able to enter the nuclei of target material. They are then able to knock out other particles, like protons, neutrons, alpha particles or heavier ions. A general sketch of the interactions can be seen in figure 2.1. Some of the new elements created could be radioactive isotopes, which will collapse at some time later. While the stopping and scattering of the protons are only able to absorb a small fraction of the total energy, nuclear interactions could transform all of the energy [19].

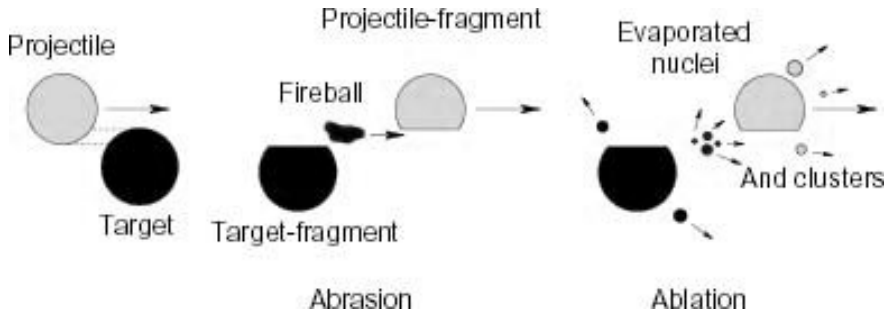

Figure 2.1: Fragmentation of a nuclei by a fast charged particle [20].

2.4 Physical absorbed dose

As the particles interacts with the target material, most of the kinetic energy is deposited through ionization of atoms. If biological matter is irradiated, the ionized molecules produced could harm the organism. The effect of the ionizations could be macroscopic quantified as the energy absorbed locally in the target material. Therefore, the physical dose is defined as the energy absorbed from the particles per mass of tissue:

$$D \equiv \frac{E}{m}. \tag{2.3}$$

Dose is measured in Gray (Gy), where $1\,\mathrm{Gy} = 1\,\mathrm{J/kg}$.

If dN particles transfers dE each passing through an infinitesimal cylinder of cross sectional area dA, thickness dl and density ρ we have

$$\frac{E}{m} = \frac{-(dE/dl) \times dl \times dN}{\rho \times dA \times dl} = \frac{dN}{dA}\frac{S}{\rho}. \tag{2.4}$$

where $\frac{dN}{dA}$ is the infinitesimal particle fluence, S the stopping power and ρ is the density of the target material.

The absorbed dose from the particles can then be written as

$$D = \Phi\frac{S}{\rho}. \tag{2.5}$$

This means that the absorbed dose D is dependent upon the fluence Φ and the stopping power S. [19].

2.4.1 The energy/range relation of Bragg curve

The characteristic depth dose distribution of ions, commonly known as the Bragg curve, as shown in figure 2.3. gets its familiar shape from these three main interactions. The shape of the ionization curve is strongly dependent on the energy of the particles. The mean range R_0 can be calculated using the Continuous Slowing Down Approximation (CSDA), by integrating over the stopping power from equation 2.2 for the maximum energy E_0 to 0:

$$R(E_0) = R_0 = \int_{E_0}^{0} \left(\frac{\mathrm{d}E}{\mathrm{d}l} \right)^{-1} \mathrm{d}E \tag{2.6}$$

$$R_0 = \alpha E_0^p. \tag{2.7}$$

where the p coefficient is dependent of the particle type and α is dependent of the absorbing medium. The International Commission on Radiation Units & Measurements (ICRU) have experimentally given $\alpha \approx 2.2 \times 10^{-3}\mathrm{cm\ MeV^{-p}}$ and $p \approx 1.77$ for protons passing through water [21]. Calculation of the relationship for protons and carbon ions are shown in figure 2.2 [19].

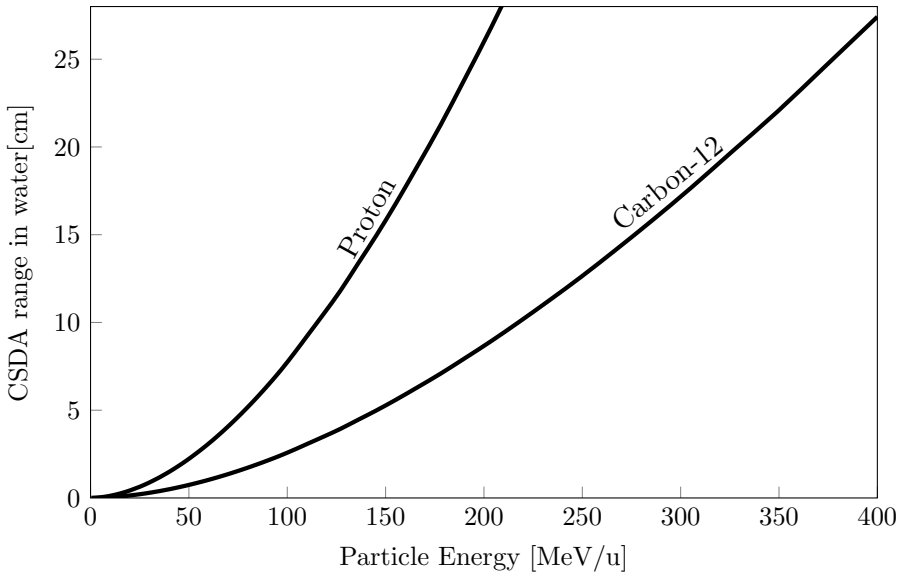

Figure 2.2: CSDA range R_0 of different particles in water, based upon the PSTAR database [22]. Calculated with Libamtrack, an online software package [23]. When fitted to equation 2.7, this calculation gives $\alpha = 0.0024\,\mathrm{MeV}^{-1}$ and $p = 1.75$ for protons and $\alpha = 0.0011\,\mathrm{MeV}^{-1}$ and $p = 1.69$ for carbon ions.

2.4.2 Range straggling

Since all of the particle interactions are random processes, the particles in a beam will not follow the exact same path. They are stopped and scattered differently, thus every particle would not have the same range in the material, even for monoenergetic particles in a homogeneous material. The range of the different particles are normally distributed, with the standard deviation σ_R. The statistical phenomenon is called range straggling, also known as longitudinal scattering. The familiar bell shape of the Bragg peak is a consequence of the range straggling. Range straggling is almost proportional to the range of particle. According to an approximation by T. Bortfeld [21], the relation is $\sigma_R = 0.012R_0^{0.935}$, for protons in water. For heavier ions, like carbon, the straggling effect is smaller. The Bragg peak is therefore narrower compared to protons with the same range [24].

2.4.3 The spread out Bragg peak

The delivery of a homogeneous dose to the whole target volume is an important principle of radiation oncology. The dose should be no less than 95% or higher than 107% than the prescribed dose, as recommend by the ICRU [25]. While conventional radiation therapy normally use rotational techniques to create a uniform dose to the Clinical Treatment Volume (CTV), protons are able to fulfil the principle from one single field. When Robert R. Wilson proposed the use of protons in cancer therapy in 1946 [26], he also described that by modulating the energy of the proton beam, making it possible to produce a uniform dose to the whole depth of the tumour, as seen in figure . The new depth dose curve fitted was later named "Spread Out Bragg Peak" (SOBP), as seen in figure 2.3.

With a finite and limited number of beam energies, it is impossible to get a completely flat SOBP. The plateau of the SOBP will always be slightly oscillating, but with good optimization the dose could be constrained within the limits given by ICRU. Due to large range straggling, a monoenergetic proton beam have a relatively wide Bragg peak. This is utilized in the creation of a SOBP, since the individual peaks could be placed at a large distance from each other, without making a highly oscillating SOBP.

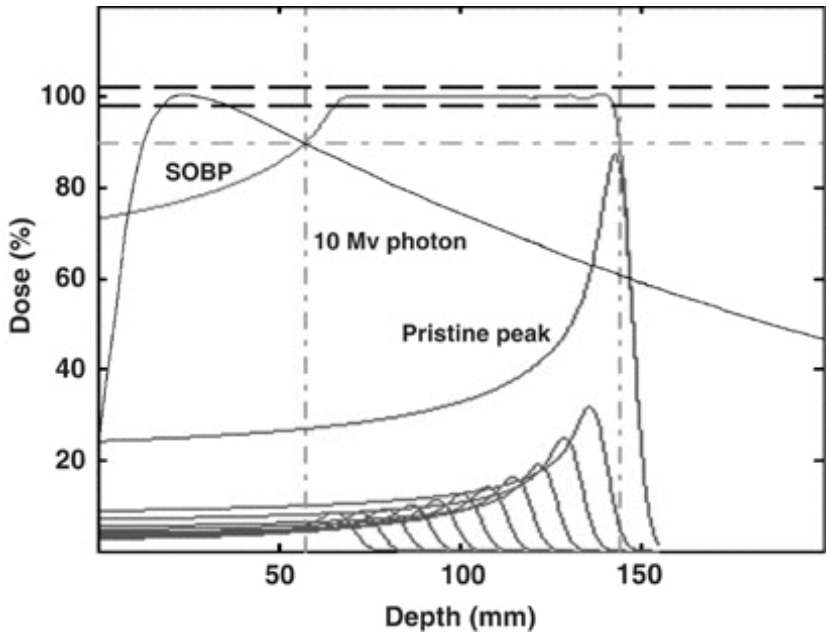

Figure 2.3: Depth dose distrubution for a proton SOBP with all its individual Bragg peaks shown. A 10 MV x-ray is also drawn for reference. The vertical lines show the relevant CTV, which is entirely covered by the single field SOBP. [27]

Carbon ions, however, have a much lower range straggling compared to protons, and hence the Bragg peak is narrower. This make it much more complicated to make a homogeneous and robust SOBP, since the distance between the individual peaks needs to be small. The number of individual Bragg peaks then becomes large, which complicates the plan and increases the treatment time. This is counteracted by the introduction a *ripplefilter* in the beam. The ripplefilter widens the energy spread of the beam before it hits the patient, which enlarges σ_R and widens the Bragg peak. The shape of the peak is then nearly similar to shape of a proton.[28]

The carbon nuclei are heavy ions consisting of multiple protons and neutrons. A fraction of the initial carbons interacts with the material, ripping of lighter ions with high energy, able to travel further than the carbon ions. They will then ionize the material behind the Bragg peak/SOBP. This region of the depth dose curve is termed the fragmentation tail.

Chapter 3

Radiation quality

3.1 Linear energy transfer

While the physical dose describes the amount of energy deposited in the media, it does not describes *how* the energy is absorbed. This also impacts the biological effect of the particles, as described in section 4. Raymond E. Zirkle introduced the term *Linear Energy Transfer* (LET), a physical quantity to overcome this problem. Zirkle defined LET as the energy transferred from the fast charged particles, per unit length of their paths, to the biological material in or near these paths [29]. Mathematically, by describing with infinitesimal units, we then achieve:

$$\mathrm{LET} \equiv \frac{\mathrm{d}E}{\mathrm{d}l}. \tag{3.1}$$

LET, due to the variations in microscopic dose deposition and the variations in the biological effect from these different dose depositions, is most convenient to measure in KeV/µm. Most of the particle's energy that is lost due to the stopping power is transferred to the target material, and deposited locally. A small portion of the energy is converted to bremsstrahlung or long range delta electrons, depositing the energy to another position in the material [30]. By assuming that all energy lost by the particles is deposited locally, we get

$$\mathrm{LET} = \mathrm{S}. \tag{3.2}$$

This is known as unrestricted LET (LET_∞) where all interactions are accounted for. This is opposite to restricted LET (LET_Δ) where interactions above a chosen energy Δ is cut off. This is done in order to exclude energy absorbed in other positions in the material, mainly deposited from high energetic delta electrons with a long range [31].

The stopping power S is dependent on the energy E of the particle, as shown in equation 2.2, which means that LET is also dependent of the energy of the particle, LET(E). In figure 3.1, the LET values (or stopping power) for protons and carbon ions passing through water are shown, with energy ranging from 0.1 MeV/u to 400 MeV/u. It is then simple to find the LET value of the beam, if one knowns the particle type and the energy, by analytical calculations or computer simulations.

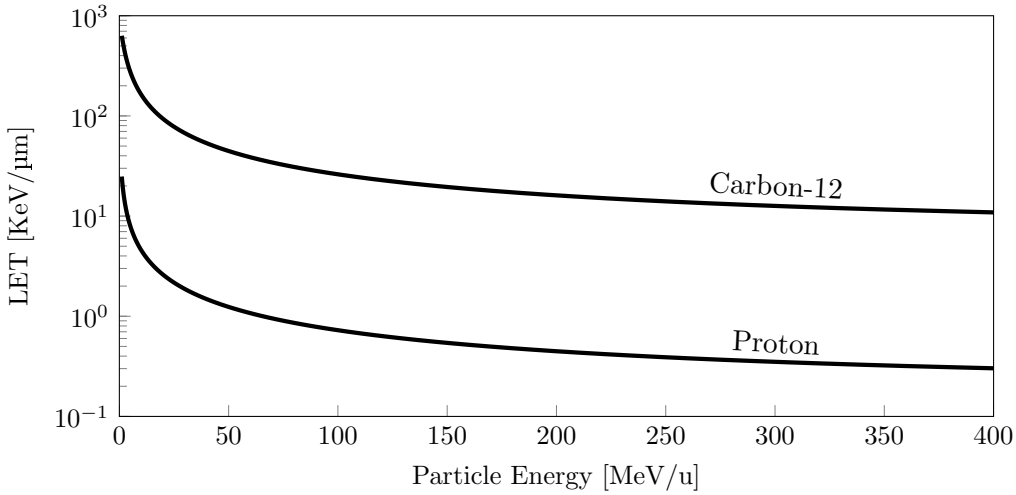

Figure 3.1: LET in water as function of energy of different particles. Calculated by The Bethe-formula, online with Libamtrack [23].

The dosemetric effect of every transfer could be found by applying the assumption from equation 3.2 into equation 2.5. We then achieve:

$$D = \Phi \frac{\text{LET}}{\rho}. \tag{3.3}$$

The dose is then linear dependent of the dosemetric value. This means that by going to higher LET particles, like carbon, fewer particles are needed to deliver the same physical dose.

3.2 Linear energy transfer spectrum

While it is simple to calculate the LET value of monoenergetic beams with a single particle type, the calculation gets more complicated in a clinical setting. Deep inside the tissue, the beam consists of multiple particle types with a range of different energies, due to range straggling and production of secondary particles, as described in section 2.4.2 and 2.3. This even occurs if the initial beam is extracted as a perfect monoenergetic beam from a synchrotron. The picture gets even more complex when analysing SOBPs, when the field consists of a broad energy spectrum, as described in section 2.4.3 [32].

A new term is therefore introduced, the *LET spectrum*. The LET spectrum is a distribution of all relevant LET values at a specific position z along the beam trajectory. The *track LET spectrum* or *fluence LET spectrum*, $f(L)$, is weighted by the fluence of the different LET values, or simply just every energy transfer passing through that position. [1] In the ICRU report 16 $f(L)$ is defined from the fraction of the fluence of particles with different L [31]:

$$f(L) \equiv \frac{\Phi(L)}{\int_0^\infty \Phi(L)\mathrm{d}L} = \frac{\Phi(L)}{\Phi}. \tag{3.4}$$

With this definition, the distribution is normalized to 1, similar to a probability distribution function:

$$\int_0^\infty f\left(L\right)\mathrm{d}L = 1. \tag{3.5}$$

As noted by Grassberger and Paganetti, the spectrum is normally not considered in radiobiological modelling, and the average values is used instead [11]. The fluence weighted LET average, LET_f, is found by the first momentum integral of the spectrum:

$$\mathrm{LET}_f = \int_0^\infty Lf\left(L\right)\mathrm{d}L. \tag{3.6}$$

One trivial example of a LET spectrum is the one made from a monoenergetic

[1] To describe the individual LET values within a spectrum, L is used instead of LET, to make a distinct difference from the averages LET_f and LET_d. Either one could have used a bar to mark the difference, $\overline{\mathrm{LET}_f}$ and $\overline{\mathrm{LET}_d}$, which is sometime used. The variable L is then an analogue to the microdosimetric variable y, described in subsection 3.3.

beam of a single particle type. The spectra then looks like a delta Dirac function:

$$f(L) = \delta(L - LET(E)) = \delta(L - S(E)), \tag{3.7}$$

where $S(E)$ is the stopping power of the monoenergetic particle with energy E, as shown in figure 3.1.

Two examples of track LET spectra $f(L)$ are shown in figure 3.2, made by a monoenergetic proton beam dropped in a water phantom. The first spectrum is measured at the entrance, and shown as a delta shaped function, since the beam is monoenergetic here. The spectrum is similar to a $\delta(L - 0.655\,\mathrm{KeV/\mu m})$.

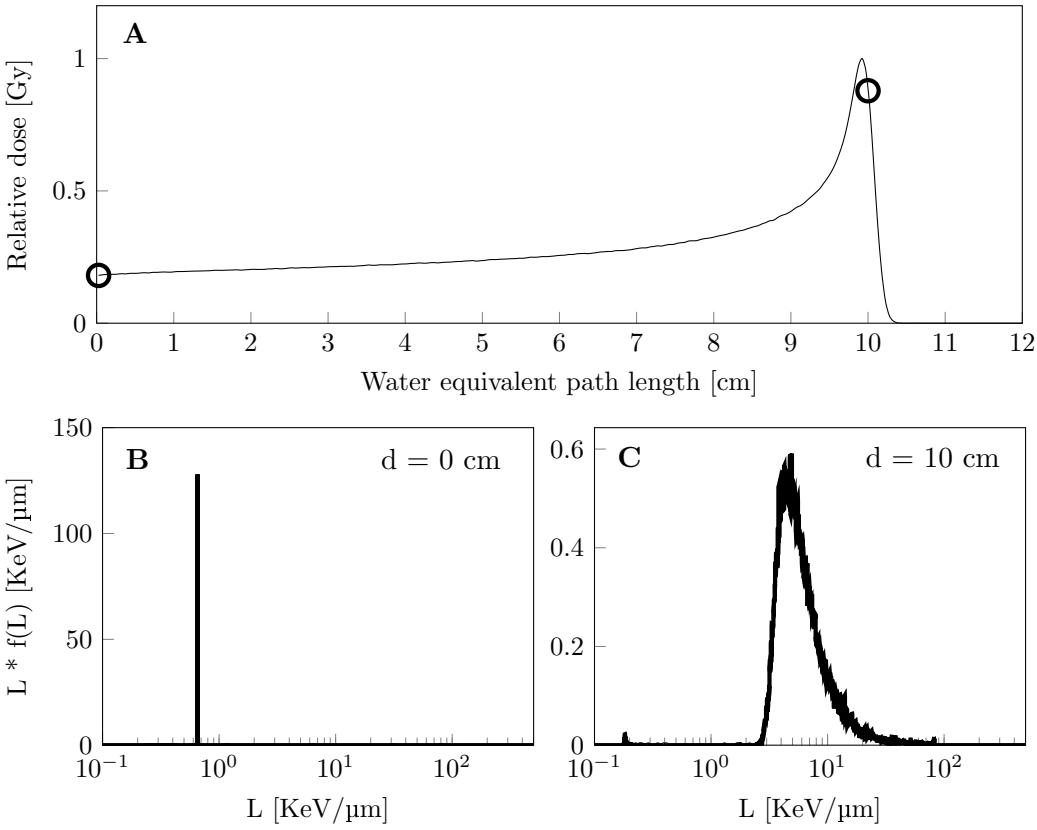

Figure 3.2: Illustration of the LET spectra $f(L)$ resulting from a 116 MeV monoenergitical proton beam in water, measured at different depths. **A** The depth dose curve of the beam. Two measured positions at the entrance (d = 0 cm) and at the distal end of the Bragg peak (d = 10 cm) are shown as circles. **B and C**: LET spectra of the beam at 0 cm (B) and 10 cm (C). The ordinate in figure B and C has been multiplied by L, which is the most common used representation for the frequency of events, according to Rossi et al. [33].

At the end of the Bragg peak the beam is consisting of multiple particles and protons with different energies, due to the range straggling effect and particle production. This can be seen in figure 3.2 C, where the spectrum is broad. The LET_f value is also shifted to higher L value, since the energy is lower, as shown in the relationship in figure 3.1.

The track LET spectrum $f(L)$ does only describe the relative distribution of different energy transfers which occurs at that position, not the the relative dose effect of the transfers. By doing a partial expansion of equation 3.3, were able to deduce the dose contribution $D(L)$ from every LET value L:

$$D(L) = \Phi(L)\frac{L}{\rho}. \tag{3.8}$$

By the use of equation 3.4 and 3.6, the total dose can then be rewritten to:

$$\begin{aligned} D &= \int_0^\infty D(L)\mathrm{d}L = \int_0^\infty \Phi(L)\frac{L}{\rho}\mathrm{d}L && (3.9)\\ &= \frac{\Phi}{\rho}\int_0^\infty L\frac{\Phi(L)}{\Phi}\mathrm{d}L && (3.10)\\ &= \frac{\Phi}{\rho}\int_0^\infty Lf(L)\mathrm{d}L && (3.11)\\ &= \Phi\frac{\text{LET}_f}{\rho}. && (3.12) \end{aligned}$$

Which is similar to equation 3.3, but this equation also hold for beams consisting of particles with several LET values. By using this equation and equation 3.8, it is possible to find the *dose weighted LET spectrum* $d(L)$:

$$\begin{aligned} d(L) &\equiv \frac{D(L)}{D} && (3.13)\\ &= \frac{\Phi(L)L}{\rho}\frac{\rho}{\Phi\text{LET}_f} && (3.14)\\ &= \frac{L}{\text{LET}_f}f(L). && (3.15) \end{aligned}$$

The dependency on the fluence LET spectrum is utilized in further analysis. Also the dose weighted LET spectrum is normalized to 1:

$$\int_0^\infty d\,(L)\,\mathrm{d}L = 1. \tag{3.16}$$

And in the same way as $\mathrm{LET_f}$, the dose average LET can be found by:

$$\mathrm{LET}_d = \int_0^\infty Ld(L)\mathrm{d}L. \tag{3.17}$$

The $d(L)$ and LET_d are weighted with the local dose, which eases the use for phenomenological radiobiological modelling. But when going to lower doses or going to higher LET values, dose weighted LET is inappropriate for characterizing the radiation quality [14]. For example, monoenergetic carbon ions of 2 MeV/u with a high LET-value of about 500 KeV/µm only six particles passing through a 10 µm x 10 µm x 10 µm volume are needed to deposit a local macroscopic dose of 2 Gy in that same volume [34]. Then the non stochastic LET_d and $d(L)$ is regarded as to uncertain to describe the radiation quality in that volume. Even the track LET would be an unstable quantity for estimating the biological effect. More analytical models like the Local Effect Model (LEM) are then needed [35]. LEM is a amorphous track structure model where the ionization radius of the delta electrons is calculated to estimate the the potential damage to the DNA. Also the sizes of the cells and nuclei should be included in track structure models. Such models are more analytical and complex, compared to simple phenomenological models.

By introducing dirac Delta equation 3.7 in equation 3.6 and 3.17, we achieve:

$$\mathrm{LET_f} = \mathrm{LET_d} = \mathrm{S}, \tag{3.18}$$

which holds for all monoenergitic particle beams. The fluence weighting average and dose weighting average are only meaningful and distinct quantities when there is a broad spectrum present [36].

Both distributions, f(L) and d(L), are independent of the absorbed dose and the dose rate. This implies that also their averages, LET_f and LET_d, are independent of the dose [37].

3.3 Microdosimetric quantities

LET is limited by the fact that is does not represent the dose deposited in a volume, only the energy, dE, transferred from a particle to the medium over a distance, dl. To overcome this, Kellerer and Rossi introduced the quantities *specific energy* and *lineal energy* [38]. The specific energy, (z_1), is the microscopic energy, ϵ, deposited from a single event in a tiny volume with mass, m. It is the microscopic analogue to dose and defined as:

$$\mathrm{z}_1 \equiv \epsilon/m. \tag{3.19}$$

and the specific energy of multiple events in the same volume is defined as:

$$\mathrm{z} = \sum \epsilon/m. \tag{3.20}$$

Specific energy is as dose measured in Gray. Lineal energy is not a straight forward analogue to LET, as specific energy is to dose. While LET is measured along the trajectory of the particle, the lineal energy, y, is defined as the energy divided by the mean chord length, $\bar{l}$, of the microscopic volume:

$$\mathrm{y} \equiv \epsilon/\bar{l}. \tag{3.21}$$

The mean chord length $\bar{l}$ is dependent of the shape and size of the volume. It could be calculated by the Cauchy formula or found in tables. A spherical volume with diameter d has the mean chord length $\bar{l} = 2d/3$. As LET can be restricted by an energy cut-off, lineal energy is restricted by a geometry cut-off, the mean chord length. The geometrical cut-off is often set such that the volume imitates the size of a cell. The the specific energy and lineal energy could be used to describe the way a single cell is impacted by radiation. Contrary to LET, the lineal energy and the specific energy are stochastic quantities, which can be measured by Tissue Equivalent Proportional Counters (TEPC). The measured spectrum is then dependent of the size and shape of the TEPC. And as the LET spectrum, the lineal energy spectrum, $f(y)$, could be dose weighted, $d(y)$. The corresponding averages could be found from the spectra (y_f and y_d). Equivalent equations then apply [33].

Chapter 4

The radiobiology of particle therapy

Conventional radiation therapy utilizes the ionizing capability of high energy γ-rays and x-rays. When energy of a photon is absorbed by the biological medium, free electrons are produced. Some of these are produced with high energy close to the DNA structure and are able to split one or two DNA strands. This process is known as direct ionization.

However, about 70 % of effect from photon therapy, is produced by so called indirect action [40]. Then the electrons are not able to hit the DNA by itself, but produces a OH - radical in a reaction with nearby water molecules. This OH - radical could, if produced close enough to the DNA, damage the DNA.

Damage due to direct action will in most cases split both DNA strands at once, creating a double strand break (DSB). This only happens rarely with indirect action, which normally only damage one of two strands, creating a single strand break

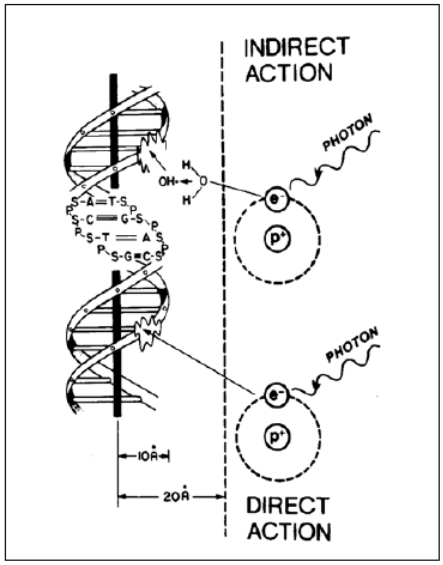

Figure 4.1: Illustration of the damaging of the DNA by ionizing action. The sketch also holds for ions [39].

(SSB). DSB are harder for the cell to repair, which makes them more effective than SSB, with respect to cell killing [39].

When transferring to ions with higher ionizing density, the electrons produced will have higher kinetic energy. Then the 70% - 30% effect distribution of indirect and direct action is shifted. Direct action is the dominant effect in therapy with protons with high LET and carbon ions. This also in practice implies that the ratio of DSB over SSB is higher for high LET particles, compared to photon therapy [40]. Ions will therefore have a higher biological effect compared to photons, if the same physical dose is given by both types of radiation.

4.1 Linear quadratic model

In 1956 irradiated Theodore T. Puck and Philip I. Marcus cultured HeLa cells with x-rays with different dose levels. They counted the number of cells N before and after irradiation, and calculated the survival fraction by:

$$S = \frac{N_{\text{after}}}{N_{\text{before}}}. \tag{4.1}$$

By plotting the survival fraction S vs. the dose D, they where able to find a survival curve with a small slope at low doses, then gradually rising towards higher doses [41]. This curve could be described by the linear-quadratic model (LQ), the leading radiobiological survival model today:

$$S(D) = e^{-\alpha D - \beta D^2}. \tag{4.2}$$

where α and β are constant parameters, which should be fitted to the experimental data for every radiation and cell type. The α and β could be coupled to the DNA damage in the cell and their repair mechanisms. At low doses, SSB are more repairable than DSB. Then the α term is dominating. While at large doses, multiple SSB occurs at the same place locally, which in practice is a DSB. But this is not a strict correlation; the α and β are simply only the best fitted values of the model to the experimental measurements.

The response of different cells can be described by the ratio $\frac{\alpha}{\beta}$. The unit of the ratio is measured in Gy, and is situated at the dose level where the α and

the β terms have the same effect. This quantity is low for radioresistant cells and normal tissue and high for cancer cells. The $\frac{\alpha}{\beta}$ ratio from photon radiation is be used to quantify the radiosensitivity of different tissues.

The radioresistant property of healthy normal tissue is the rationale behind fractionation of the treatment. The radiation is then given at small doses, typically 2 Gy per day, divided over 20-40 days. The gain from fractionation is reduced for carbon ions, which enables the possible cut down the number of fractions. In the most extreme version of hypofractionation in carbon ion therapy, only one single fraction dose is given to the patient [42].

4.2 Relative biological effectiveness

Radiation therapy with protons and heavy ions are based upon the empirical knowledge in treatment with photons. However, heavy charged particles do not interact with the tissue in the same manner as photons, thus the treatment protocols cannot be used directly and have to be translated. Today, this translation is done by introducing the *Relative Biological Effect* (RBE). RBE is defined as the ratio between the photon reference dose and the ion dose, yielding the same biological effect:

$$\text{RBE}(endpoint) \equiv \frac{D_{reference}}{D_{ions}}. \tag{4.3}$$

The RBE could then be used to find the biological effective dose (BED) of the particle beam [43] [44]. This is found by

$$\text{BED} = \text{RBE} \times D. \tag{4.4}$$

which is measured in Gy(RBE). The BED of the particle radiation should then make the same biological impact as similar physical dose from the reference photon radiation. The biological endpoint is chosen by the user to translate the dose from the particle to a photon dose, by the RBE value. In general, the biological endpoints should be quantifiable and simple to measure, such as intestinal crypt regeneration, foci formations or chromosome aberrations [14]. But

the most common used endpoint is the survival fraction of the cells. It is then possible to model the RBE as a function of the dose either the survival fraction S or the reference dose level D_x, by setting

$$S_{\text{ions}}(D) = S_{\text{reference}}(D_x), \tag{4.5}$$

where

$$S_{\text{ions}}(D) = e^{-\alpha D - \beta D^2} \qquad S_{\text{reference}}(D_x) = e^{-\alpha_x D_x - \beta_x D_x^2}. \tag{4.6}$$

where α and β are the LQ parameters of the ion radiation and the α_x and β_X are the LQ parameters of the photon reference radiation.

As an example, two survival curves for protons and x-rays irradiating V79 hamster cells are shown in figure 4.2. The response is higher for the protons relative to the photons, thus the curve is initial steeper. This gives a RBE of 2.29 at an reference dose of 2 Gy. While at 8 Gy the relative difference is smaller, only 1.43. In general, the RBE is high for lower fraction doses and low at high fraction doses.

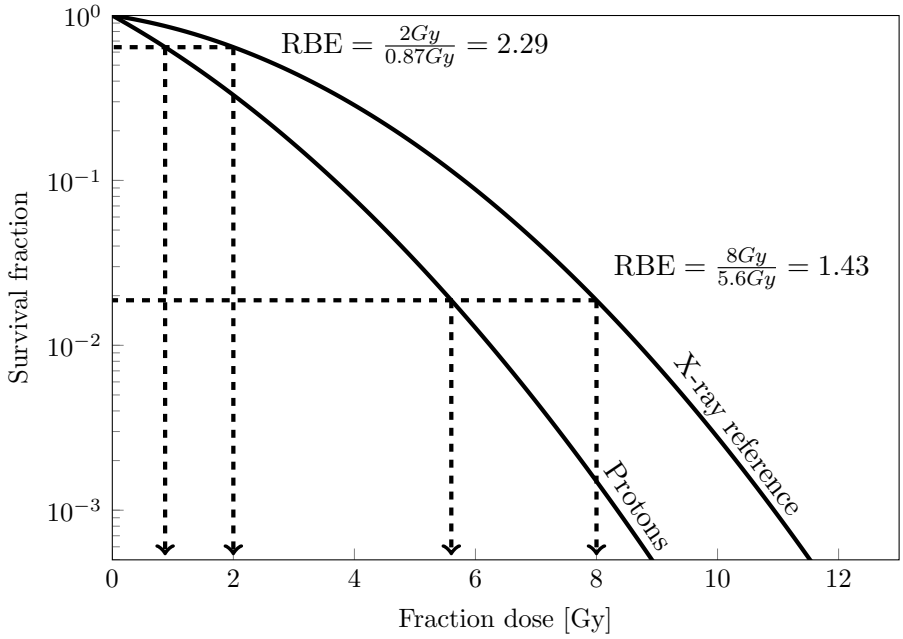

Figure 4.2: Schematic dose response curves of irradiated V79 hamster cells, irradiated with monoenergetic protons with a mean LET_d= 20 KeV/µm and with reference X-rays. The α and β data originates from Belli et al [45].

By assuming the continuous relationship between survival and dose from the linear-quadratic model, we can find a function for RBE dependent of the reference dose D_x. This is done by solving equation 4.5 by setting D_x as the undetermined variable. We then achieve:

$$\mathrm{RBE}(D_x) = \frac{D_x}{D} = \frac{2\beta D_x}{-\alpha + \sqrt{\alpha^2 + 4\beta\left(\alpha_x D_x + \beta_x D_x^2\right)}}. \tag{4.7}$$

If β is set to 0, the equation is then:

$$\mathrm{RBE}(D_x) = \frac{D_x}{D} = \frac{\alpha}{\alpha_x + \beta_x D_x}. \tag{4.8}$$

4.3 RBE dependency on radiation quality

The RBE is not only dependent on fraction dose, but also the fraction regime, the tissue type, the particle type and the radiation quality. When the radiation is shifted towards higher LET, more direct ionization occurs and DSB dominates over SSB. This changes both the α and the β parameters of the linear quadratic model. For high LET radiation, the β could be considered negligible and set to 0. The effect of different magnitudes of LET in a carbon ion beam can be seen in figure 4.3. In this example, the survival curves loses their shoulder and get steeper as the LET value increases. This effect is similar also for protons.

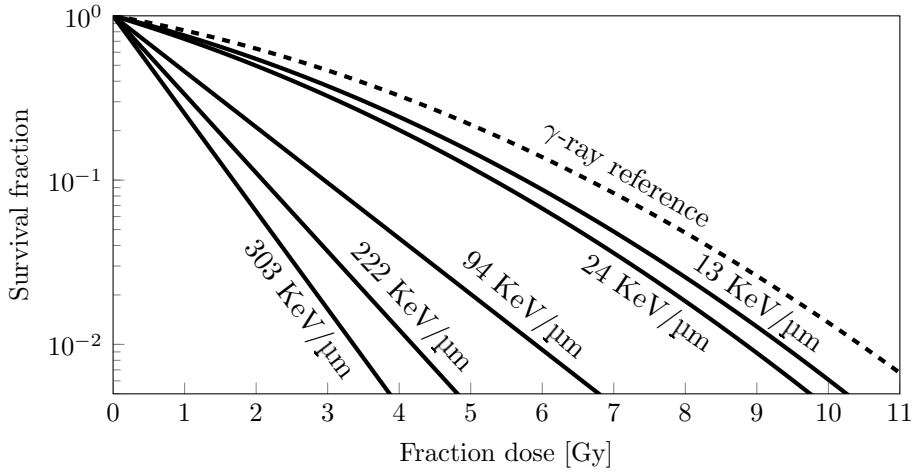

Figure 4.3: Schematic dose-response curves of irradiated V79 hamster cells, irradiated with monoenergetic carbon ions with different LET_d and γ-rays. Data from Belli et al [46].

As α and β need to be deduced by fitting experimental data, there is no general formulation of the LET dependent α(LET) and β(LET). But Furusawa et al. and others have made a comprehensive work in experimenting with different cell lines and different LET values [47]. The tabulated α and β made by Furusawa et al. are the radiobiological basis of the old Japanese algorithm for estimation of the RBE in carbon ion therapy [48].

Many others have also performed cell survival experiments with different particles, LET values and tissue types. Friedrich and colleagues at GSI, Darmstadt have collected over 850 cell experiments from 77 different papers, and published them in an open database [13]. The database consists of all experiments since the seventies with ions from protons to uranium. In a review article from fall 2014, Harald Paganetti also published data of cell experiments with protons [14]. Both of these databases include the α, β and LET_d/LET of the particle survival curve, as well as the α_x and β_x of the reference radiation. By combining these databases, it is possible to find a global RBE dependency of LET_d. This is done by solving equation 4.7 or 4.8 for every single experiment, and plotting the RBE as function of the tabulated LET_d. In figure 4.4A the reference dose D_x was set to 2 Gy, while in figure 4.4B D_x was set to 8 Gy. Mark the dependency on the fraction dose at the height and the vertical spread of the scatter plot.

Even though there is a great vertical spread in the data in both examples in figure 4.4, it is still possible to spot a dependency on LET for RBE. For LET values below 10 KeV/µm, the RBE is between 1 and 2 for both. This is reasonable, since the reference radiation, either γ-rays or x-rays have a LET_d of about 1 KeV/µm and RBE of 1.

In both diagrams the relationship goes towards a peak around 100-200KeV/µm, where the relative effect is at it greatest. This peak then represent the optimal radiation quality for killing. After peaking, the RBE is falling once again. This is due to an overkill effect. The particles are ionizing too densely, such that the DNA molecule is already damaged.

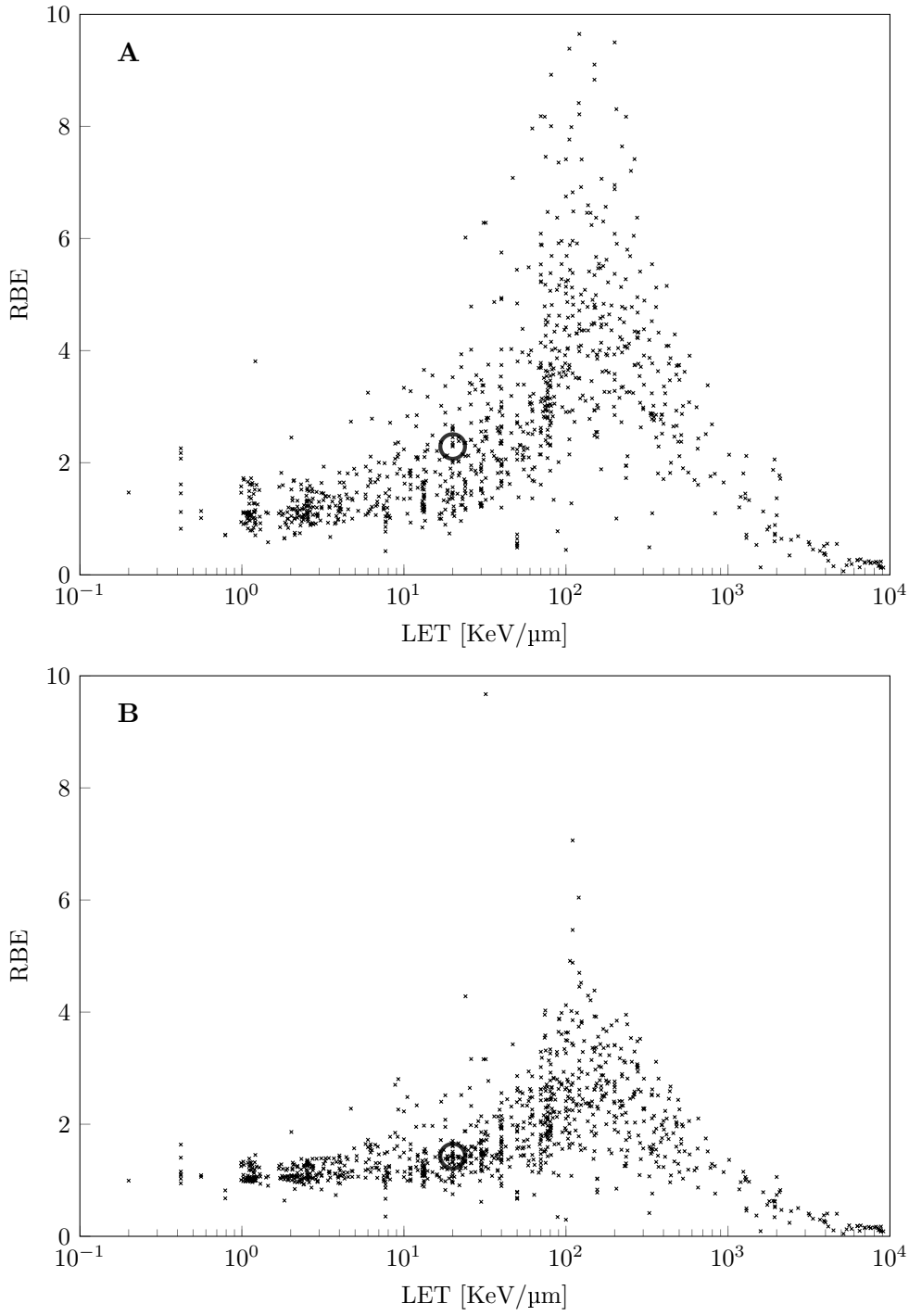

Figure 4.4: The RBE plotted against the LET_d for about 1135 experiments with LET_d between 0.1 KeV/µm and 1000 KeV/µm. In the figure A, the reference dose D_x was set to 2 Gy, while D_x was set to 8 Gy in figure B. For orientation, the light gray circles shows the 2 and 8 Gy examples from figure 4.2. Data from Friedrich et al. and Paganetti [13, 14]

4.4 Biological weighting function

By knowing the empirical relationship between LET and RBE it would be possible to use this data to create a purely phenomenological calculation model. For the LET_d range of protons, between 0 and 15 KeV/µm, Paganetti assumes that relationship is more or less linear [6]. In his 2014 review, he fits multiple different subcategories of the proton database to the function

$$\mathrm{RBE}(\mathrm{LET}_d) = A \times \mathrm{LET}_d + B, \tag{4.9}$$

where A and B are the best fitted constant to the data. Other models also assume a linear relationship of the average LET_d, but they calculate the α and β parameters instead [49, 50, 51]. Calculating the LET_d and relating the RBE as a function of LET_d is the most straight forward method to calculate the RBE, even though if the relationship is not linear.

Knowledge on the LET dependence of the RBE comes partly from the experience with fast neutron therapy. In an article from 1993 by Thomas Blue et al. on RBE in neutron therapy, they suggest the possibility of fitting clinical appropriate LET-RBE relationship to a fourth-order polynomial [52]:

$$\mathrm{RBE}(L) = a_0 + a_1 L + a_2 L^2 + a_3 L^3 + a_4 L^4, \tag{4.10}$$

where the constants a_0 to a_4 are only constant for a chosen reference dose level, D, or a chosen survival level, S. According to Blue et al. [52], the polynomial should hold for all relevant LET values below 100 KeV/µm.

The concept of biological weighting function (BWF) was widely used in neutron therapy [53, 54]. The BWF is written as a function of the lineal energy, as $r(y)$. It was used to weight the different values in the dose weighted lineal energy spectrum, $d(y)$. The RBE could then be estimated by the equation:

$$\mathrm{RBE}_{\mathrm{spectrum}} = \int_0^\infty r\,(y)\, d\,(y)\, \mathrm{d}y. \tag{4.11}$$

The most used BWF, compiled by Loncol et al, is shown in figure 4.5 [53]. The method of weighting the lineal energy spectrum was also used in proton therapy research in the 1990s [55] and still is used today [56].

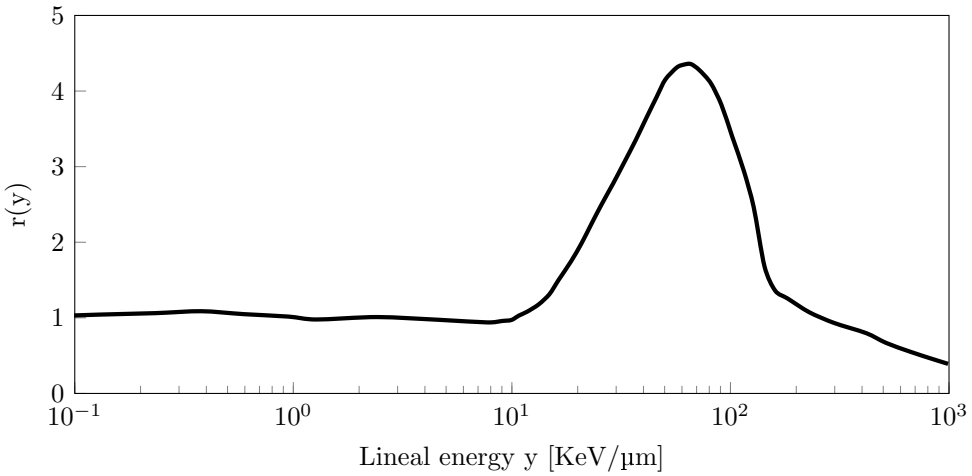

Figure 4.5: A biological weighting function based upon multiple experiments with mice irradiated with neutrons, protons and photons at different centres. Intestinal crypt regeneration in mice was set as biological endpoint. Effect after a single fraction with 8 Gy. Mark that the variable at the x-axis is the microdosimetric quantity y. Redrawn after Loncol et al.[53]

Chapter 5

Method and Materials

5.1 Summary of method

In this thesis, the concept of BWF is adapted from the realm of microdosimetry and lineal energy spectrum, to the LET spectrum. By rewriting equation 4.11 we then achieve:

$$\mathrm{RBE}_{\mathrm{spectrum}} = \int_0^\infty r\left(L\right) d\left(L\right) \mathrm{d}L. \tag{5.1}$$

Further, a pseudo BWF was created by assuming as Blue et al., that a fourth-order polynomial to experimental data would do, not only up to 100 KeV/µm, but to 1000 KeV/µm. We then achieve the following BWF:

$$r(L) = a_0 + a_1 L + a_2 L^2 + a_3 L^3 + a_4 L^4, \tag{5.2}$$

where a_0 to a_4 is dose dependent constants. Experimental data was collected from two databases [13, 14]. The RBE value calculated by "the spectrum method" should then be found by equation 5.1, and the corresponding BED by equation 4.4.

The BED of "the spectrum method" was then compared to the BED of the "the average method". The latter was found by finding the LET_d, and simply using this as input in the BWF instead:

$$\mathrm{RBE}_{\mathrm{average}} = r\left(\mathrm{LET}_d\right). \tag{5.3}$$

The same BWF of equation 5.2 is used in both methods, for simplified comparison of the two calculation methods.

Monte Carlo calculations were performed with FLUKA [57, 58], by simulating a total of four treatment beams: Two different beam setups for both protons and carbon ions; one monoenergetic setup and one SOBP setup. The latter gave an homogeneous dose in a predefined volume. The beams were dropped in a water phantom, where the dose D and fluence LET spectrum $f(L)$ were measured at different depths z. At 50 different positions, the D and $f(L)$ were then used to estimate the $\text{RBE}_{average}$ and the $\text{RBE}_{spectrum}$, and hence the BEDs. This summary of the method can also be seen graphically in figure 5.1.

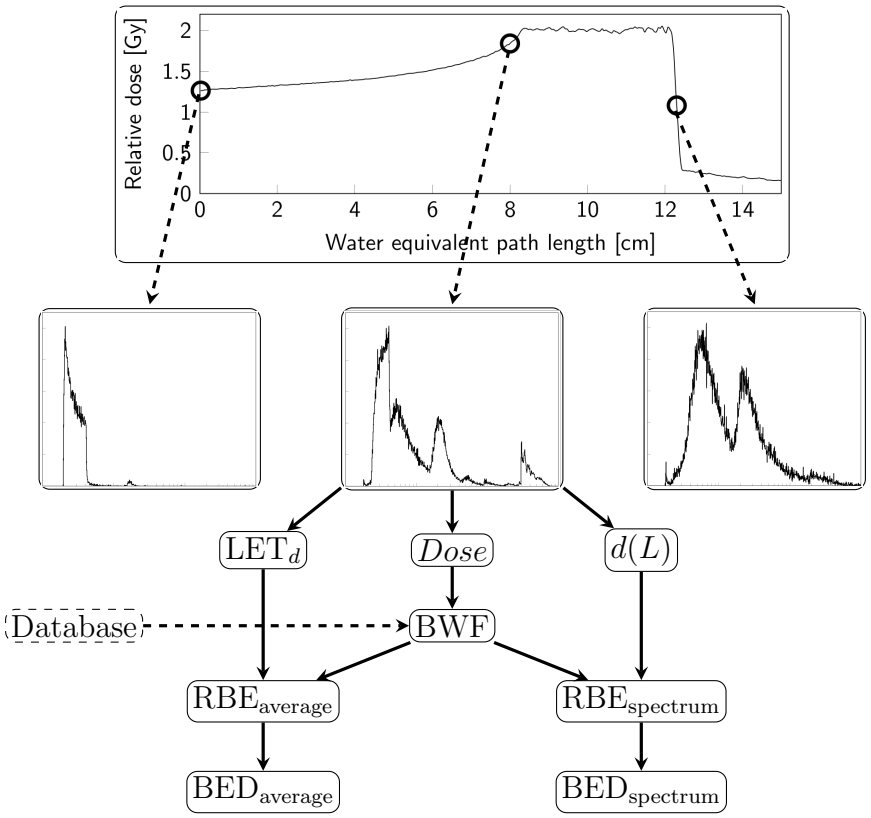

Figure 5.1: Schematic diagram of the methodology in this thesis. The LET spectra are found at 50 different depths; three examples are shown here. The physical dose, the dose weighted LET average and dose weighted LET spectrum are found at every position. A dose dependent BWF, based on a database of cell experiments is used to find the RBE for both methods at that specific position. The BED could then be found. For protons, the BED with an RBE=1.1 is also calculated, but this is not shown.

5.2 Beam definitions

To imitate a general and realistic clinical setup, the SOBP was set to cover a depth from 8 to 12 cm from the phantom surface. The same definition of target volume depth is also used as an example by others [59, 60]. Ytre-Hauge provided optimized proton and carbon treatment plans made with TRiP [61]. TRIP is a heavy ion treatment planning software (TPS) developed at GSI, Darmstadt [62]. Bassler provided a source.f file and python script to adapt the energies and the weighting from TRiP to the FLUKA environment [59]. The script is shown in appendix A. For the carbon plans, the oscillations in the SOBP are too large, therefore a ripplefilter is needed to smoothen out the individual Bragg peaks, as discussed in section 2.4.3. This was implemented in FLUKA by adding a custom script, also provided by Bassler [59].

For the setups with monoenergetic beams, the particle energies was set to the same energy as the last pristine Bragg peak of the SOBP, which corresponds to a range of about 12 cm. The energy spread, σ_E, was set to be 0.1%, similar to a optimized synchrotron beam [63]. The lateral focus, σ_x and σ_y were set to be 10 mm, a reasonable width [64].

The carbon setup was initialized with one million particles. In order to achieve similar statistics for the proton runs, ten million primary particles were simulated. Since the $d(L)$ and LET_d are independent of the absorbed dose, there is no need to simulate a fraction dose of 2 Gy.

5.3 Scoring

5.3.1 Dose

The dose in the water phantom was logged in cylindrical volumes, with a height of 0,5 mm along the z axis and a radii of 1 cm in the xy plane. The depth dose curves were then normalized to 2 Gy, by two different methods. For the individual Bragg peaks, the highest point of the Bragg peaks were normalized to 2 Gy, and the rest were related to this dose. While in the case of the SOBP curves, the mean of the scored values within the region of the PTV (between 8 cm and 12 cm) were found, and the full curve was normalized to this value. This is not a

clinical perfect normalization, according to the definition given at MGH [65]. But this normalization holds for the comparison done in this thesis.

5.3.2 Linear energy transfer

The track LET spectra $f(L)$ were scored at 50 different positions along the trajectory of the particles, as shown in figure 5.2. At the plateau region the distance between every measurement was 5 mm. Within the SOBP, the measuring frequency was increased to every 2 mm, until the distal part where the spectra were logged every 1 mm. This was done for the full distal falloff as well, before the frequency returned to every 5 mm for the fragmentation tail. The planes can be seen as the vertical lines in figure 5.2.

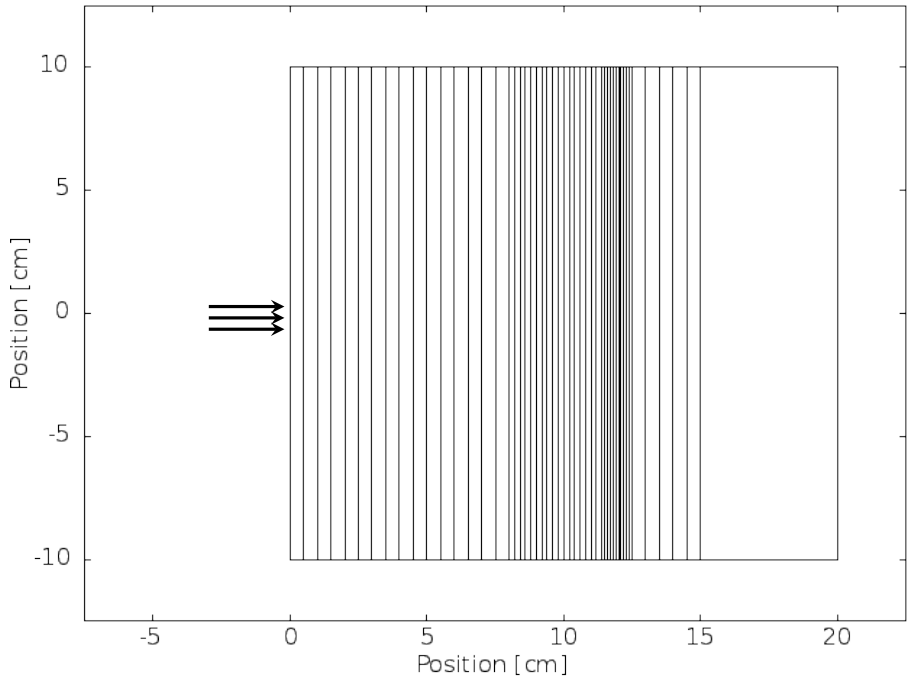

Figure 5.2: Overview of the geometry in the simulations. The beam is illustrated as the arrows to the left and the water phantom is the rectangle. The lines in the water phantom represent the planes where the fluence LET spectrum $f(L)$ is measured.

The LET spectra were scored by using the USRYIELD card in FLUKA. The parameters were set such that FLUKA scored LET from all particles in 1000 different bins, with logarithmic increasing width from 0.1 to 500 KeV/µm. The

lower and upper LET cutoff values were set to include more than 99% of the interactions at all considered positions.

By using this method, the spectrum was discretized from $f(L)$ to $f(L_n)$, where L_n corresponds to the mean value of bin number n. The same bin has width $(\Delta L)_n$.

The scoring is then made such that the normalization in equation 3.5 still holds, even though the binning is not infinitesimal:

$$\sum_{n=1}^{1000} f(L_n)(\Delta L)_n = 1 \tag{5.4}$$

Since the FLUKA is scoring the LET values as a intensity histogram in bins with finite and distinct width, also equation 3.6 needs to be rewritten as a finite sum:

$$\mathrm{LET}_f \approx \sum_{n=1}^{1000} L_n f(L_n)(\Delta L)_n \tag{5.5}$$

The LET_f value is then used to find the dose probability density, $d(L)$, and hence the dose-average LET_d. This is done computationally by first rewriting equation 3.15:

$$d(L_n) = \frac{L_n}{\mathrm{LET_f}} f(L_n) \tag{5.6}$$

By using this renormalized dose weighted LET spectrum, we find our average LET_d by rewriting equation 3.17:

$$\mathrm{LET}_d \approx \sum_{n=1}^{1000} L_n d(L_n)(\Delta L)_n \tag{5.7}$$

These equations were implemented into a MATLAB script, as shown in appendix B.

5.4 BED calculation

5.4.1 RBE modelling

Two different databases of cell experiments were found and combined. The PIDE database [13] includes over 850 different experiments with different ions, and the "Paganetti" database [14] includes more than 300 experiments with protons. Data presented in both databases were only considered once. The α and β parameters of the different experiments were used in equation 4.7 and 4.8. The local physical dose D, as read by FLUKA and normalized to 2 gray, was used as the reference dose D_x in the equations. This process was done for all 50 different readout points for the fluence LET spectrum, creating 50 different scatter plots.

From a single scatter plot, a curve was fitted to the data to create the BWF. Two primary methods of fitting the BWF to the data were used, described underneath. The following assumptions were made for the BWF to hold:

- The energy transferred from the particles to the medium is deposited locally. This neglects the presence of long range delta electrons and bremsstrahlung, thus we can assume $\text{LET} = \text{LET}_\infty = S$.
- The empirical and macroscopic RBE-LET model is sufficient for all LET values. The $d(L)$ and LET_d are seen as an acceptable representation of the radiation quality, even for high LET values at low clinical doses.
- The linear quadratic model still holds at low fraction doses.
- The cells in the experiments were irradiated with a monoenergetic beam, such that the LET spectrum equals a delta spectrum $\delta(L - \text{LET}_d)$. We could then assume that $r(L)$ is a true BWF, where every LET value L will give the biological effect of that LET value.
- The PIDE database consists of different particles. No differentiation was done, as we assume that all ions with the same LET value inflict the same biological effect. This is also debated by Sørensen et al. [66].
- The databases consist of different experiments with multiple cell lines. No differentiation of the α/β ratio was done, so the BWF is a general representation, based on the average from all available data. A similar assumption

is done at the old radiobiological model of NIRS. The model is solely based upon the in vitro response of Human Salivary Gland cells, and as that the cell line should represent the effect of all tissue [48].

- The database made by Paganetti also includes some in vivo experiments. These are not excluded, thus the effect of irradiating cells in vivo and in vitro is assumed no major differences.

Full LET range fit

The assumption by Blue et al. that a fourth order polynomial should hold was used, but extended from a max LET limit of 100 KeV/µm to 1000 KeV/µm. We then obtain a dose dependent BWF as in equation 5.2. The regression fitting was done in MATLAB with the function *polyfit*. This method can be seen in Appendix B.

Dog leg fit

As seen later in the results, the full fit BWF probably gave a bit too large RBE values for low LET values when compared to the example BWF by Loncol et al. in figure 4.5. Here the RBE value is 1 until around 10 KeV/µm. The LET dependent quality factor defined in ICRP report 60 is constant 1 below 10 KeV/µm, where it increses along as LET increases [67]. This possible configuration of the BWF could be utilized in the new model, by constraining the fit of the BWF curve to start at 10 KeV/µm with an RBE of 1. Below this value, the RBE value is constant 1. The extra BWF is of special interest for the proton beams, therefore only the proton beam setups were compared with the corrected BWF. The new BWF is nicked the "dog leg fit", after its sharp bending shape. This code is not appear in the appendix as it is only a small difference from the other BWF curve fitting script.

5.4.2 BED estimation

Three different estimations of the biological dose were done. All of the following equations were implemented into the MATLAB script in appendix B, where they calculated the different BED for every plane and every setup.

By LET spectrum

From the polynomial regression, we achieve the BWF, $r(L_n)$. This is used to calculated the RBE by the use of equation 5.1. This is done numerically by rewriting it to:

$$\mathrm{RBE}_{\mathrm{spectrum}} \approx \sum_{n=1}^{1000} r\left(L_n\right) d\left(L_n\right) \left(\Delta L\right)_n \tag{5.8}$$

The RBE value is then used to calculate the BED of the spectrum method, by multiplying it by the local physical dose D:

$$\mathrm{BED}_{spectrum} = D \times \mathrm{RBE}_{spectrum} \tag{5.9}$$

By dose average LET

The average calculation method also needs to be discretized in the same way as the spectrum method. From equation 5.3 we get:

$$\mathrm{RBE}_{average} \approx r\left(\mathrm{LET}_d\right) \tag{5.10}$$

with the representative BED value:

$$\mathrm{BED}_{average} = D \times \mathrm{RBE}_{average} \tag{5.11}$$

By constant RBE

Also, as a comparison, we add a constant RBE value of 1.1 for the proton setups. This gives us the last dose estimation:

$$\mathrm{BED}_{1.1} = D \times 1.1 \tag{5.12}$$

Chapter 6

Results

6.1 Physical dose and LET distributions

The physical doses scored in the water phantom in all four setups are plotted in figure 6.1 and 6.2 together with LET_f and LET_d. The relative dose and the LET spectrum is both independent of the dose, therefore should these figures are general for all dose levels.

According to Paganetti [14], the LET_d should be between 2 and 3 KeV/µm in the middle of a proton SOBP. This correlates good with the LET_d in figure 6.1 B. The full LET spectra $d(L)$ for protons, not shown here, have a maximum LET value at about 50-60 KeV/µm, when 99 % of the fluence is accounted for. The LET spectra from carbon ions reaches all the way to about 460-480 KeV/µm, when 99 % of the fluence is accounted for. The maximum value is found at the peak of the Bragg peak, where the LET_d is the greatest.

The LET_d is not monotonically increasing beyond the distal dose fall off in figure 6.1 B. Beyond this the proton fluence is low, such that the statistical fluctuations are large. The deposited dose is anyway low, as protons do not leave a fragmentation tail. The BED is then also negligible, independent of the RBE at this depth. There are still some minor fluctuations specially for LET_d, as seen around 3 cm depth for the proton curve in figure 6.1 B and in both of the multi-energetic curves around the proximal SOBP. Some of these fluctuations were lost for the proton curves when transferring from 1 000 000 initial particles to 10 000 000 initial particles. By simulating even more, it is thought that the LET_d depth

distributions will converge against a smooth curve at the end. FLUKA does not provide the error of the simulations with their the USRYIELD card. LET_f and LET_d should in principle anyway converge against the real value. With 10 million particles the uncertainty should be under 1% for a simple simulation like this.

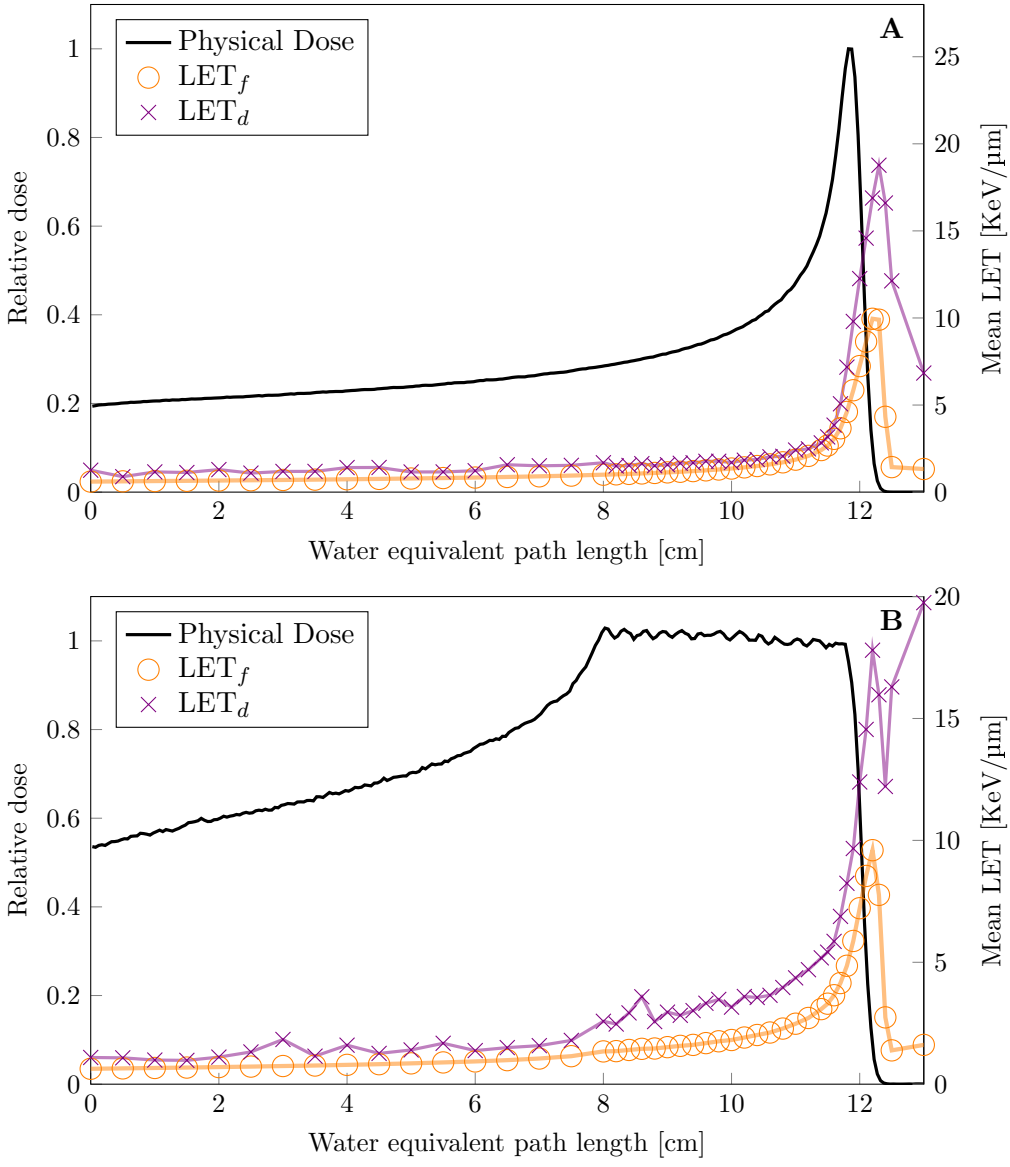

Figure 6.1: The relative physical dose and average LET quantities of a monoenergetic proton beam (A) and a SOBP proton beam (B), plotted against the depth of a water phantom. The dose is logged for every half millimeter with the intensity given at the left axis. The LET values is logged at every cross or circle with the corresponding value at the right y-axis.

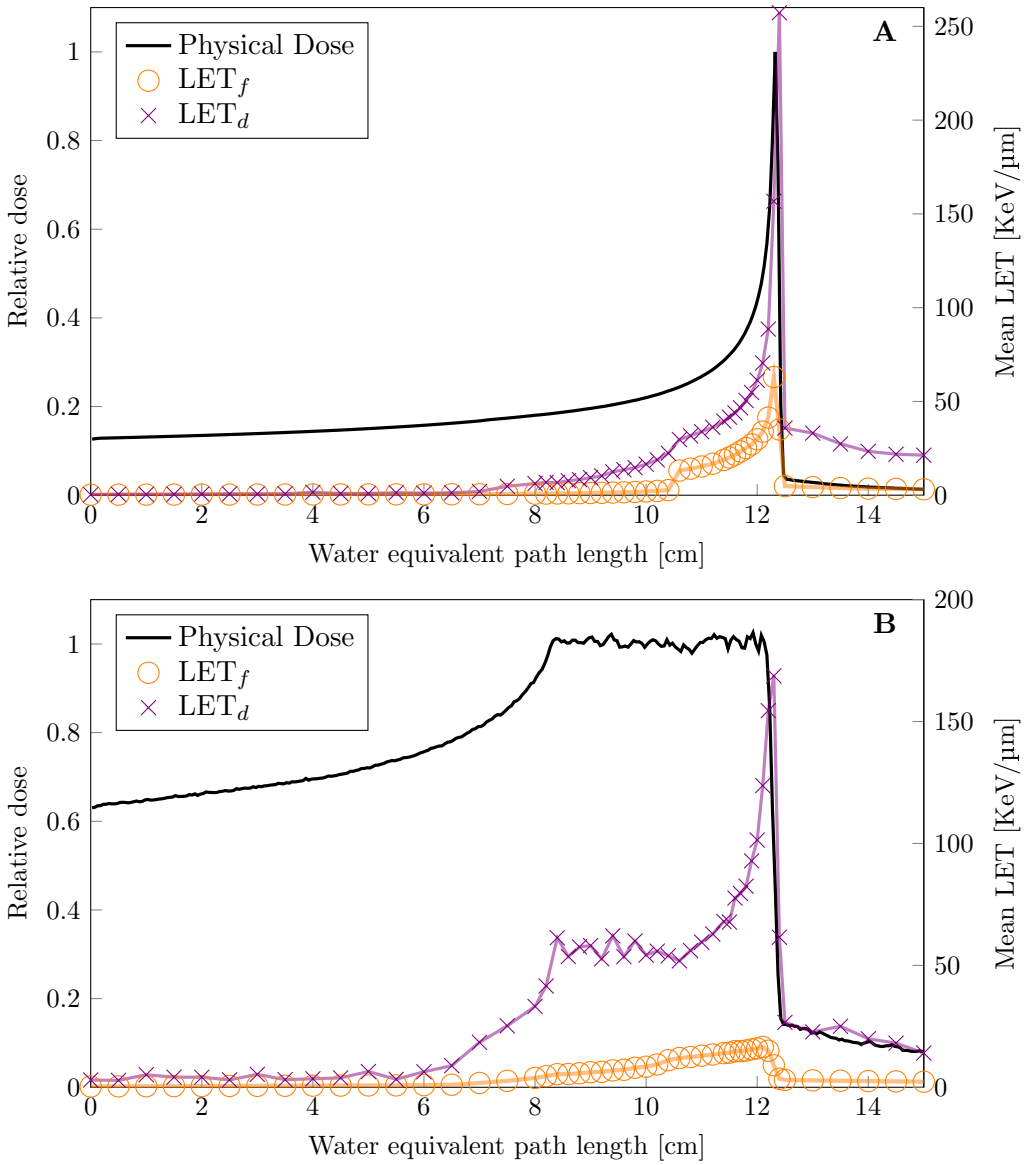

Figure 6.2: The relative physical dose and average LET quantities of a monoenergetic carbon ion beam (A) and a SOBP carbon ion beam (B), plotted against the depth of a water phantom. The dose is logged for every half millimeter with the intensity given at the left axis. The LET values is logged at every cross or circle with the corresponding value at the right y-axis.

6.2 Biological dose estimation

6.2.1 Full LET range fit

Ten different BWF curves, fitted to the RBE values calculated from the databases are shown in figure 6.3. They show the variation of RBE with dose for the range between between 0.2 Gy and 2 Gy, with a isodose distance of 0.2 Gy. The RBE increases as the local dose decreases, as also seen in the scatter plots in figure 4.4. These BWFs, or rather the continuous set of BWF, are then used to calculate the BED distributions shown for protons in figure 6.4 and for carbon ions in figure 6.5.

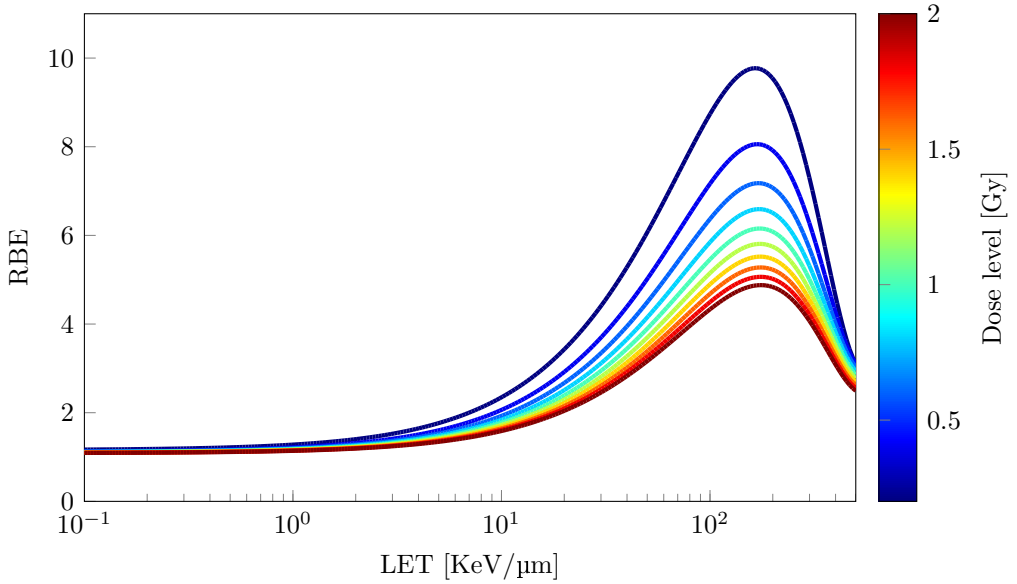

Figure 6.3: RBE as function of LET and dose. 4 order polynomial fit between 0.1 KeV/µm and 1000 KeV/µm. The BWF is limited to the relevant area between 0.1 and 500 KeV/µm. The dose dependency is in principle continuous, but only the discrete lines for every 0.2 Gy between 0.2 and 2 Gy are shown here.

Protons are particles with relatively low LET value, far below the BWF peak at around 100-200 KeV/µm. The RBE is therefore increasing monotonically along with the rising LET value. And as seen in figure 6.1, also the LET_d value increases somewhat along with depth. The RBE should therefore rise along with the treatment depth. This results in an enlarged Bragg peak for the monoenergitic proton beam shown in figure 6.4 A and in a non homogeneous SOBP, as shown in figure

6.4 B. The RBE is high toward the distal end of the SOBP and the distal dose falloff. At the maximum, the RBE is approximately 1.5, yielding a BED of about 3.0 for both examples.

The difference between the two calculation methods is minor. The ratio $\text{BED}_{spectrum}/\text{BED}_{average}$ is above 98% in all regions, besides in the distal dose fall off. At its maximum, the ratio falls to 95% in distal dose falloff. But the BEDs estimated by a variable RBE are at all depths higher than the BED calculated by a constant RBE of 1.1.

Carbon ions have much higher LET values compared to protons. In the monoenergetic carbon example the LET_d peaks above 250 KeV/µm, while the SOBP example has its maximum at almost 180 KeV/µm, as seen in figure 6.2. Both of these values are just above the peak of the BWF. The RBE is maximum when calculating with the average method, as the LET_d reconciles with the peak in the BWF. While calculating the RBE by the spectrum method, The RBE is significantly lower. As the beam consist also of portions of low LET and extreme high LET, both regions yielding relative low RBE. This causes the a great difference between the two calculation method for carbon ions. This can especially be seen along the SOBP in the second example in figure 6.5, where the RBE calculated by the spectrum method is 11-15 % below the RBE calculated by the average method. The difference is even larger in the distal dose falloff. The ratio $\text{BED}_{spectrum}/\text{BED}_{average}$ gets as low as 50% for a single position in the distal dose falloff in the SOBP example. But in other regions, the calculation differences are only minor.

The $\text{BED}_{average}$ oscillations in the SOBP in figure 6.5 are inherited from the same LET_d oscillations in 6.2.

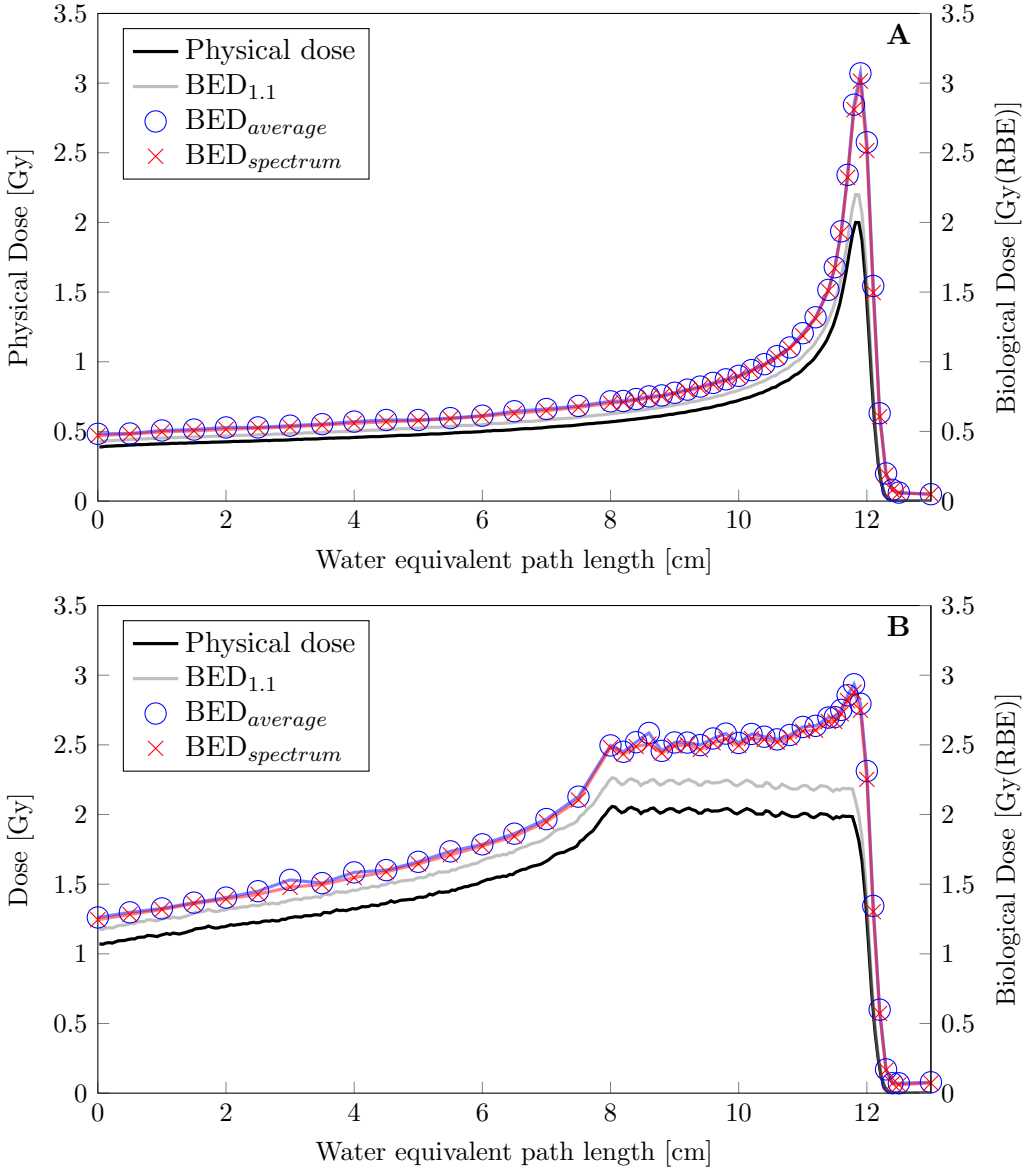

Figure 6.4: The depth dose curves of the proton setups. The BEDs are based on the full fit BWF are plotted together with the constant RBE of 1.1. **A:** The monoenergetic setup. **B:** The SOBP setup.

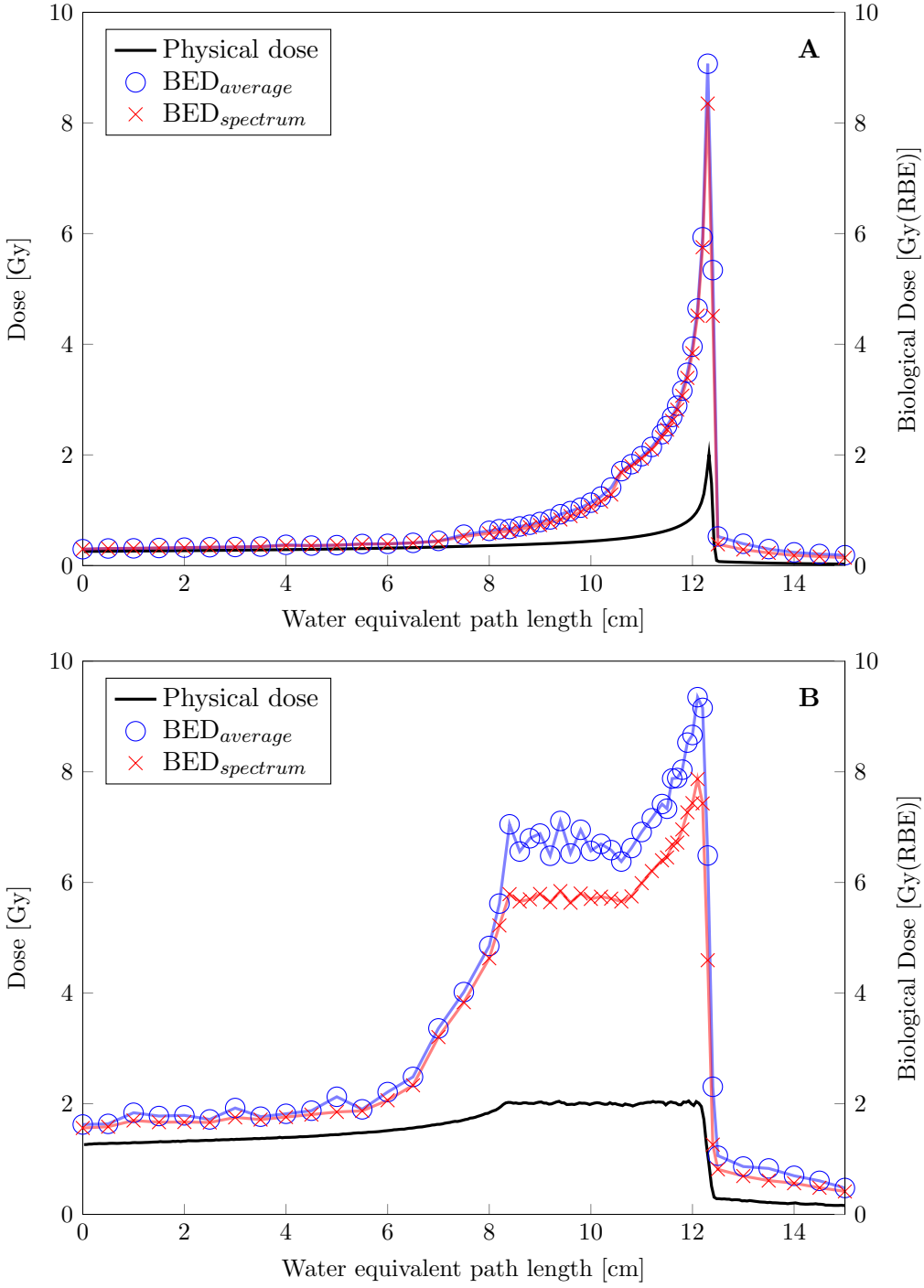

Figure 6.5: The depth dose curves of the carbon setups. The BEDs are based on the full fit BWF. **A:** The monoenergetic setup. **B:** The SOBP setup.

6.2.2 Dog leg fit for protons

The constrained BWF is shown in figure 6.6. As seen, the RBE is 1 for all doses below 10 KeV/µm, similar to figure 4.5 and the ICRP 60 quality factor [53, 67].

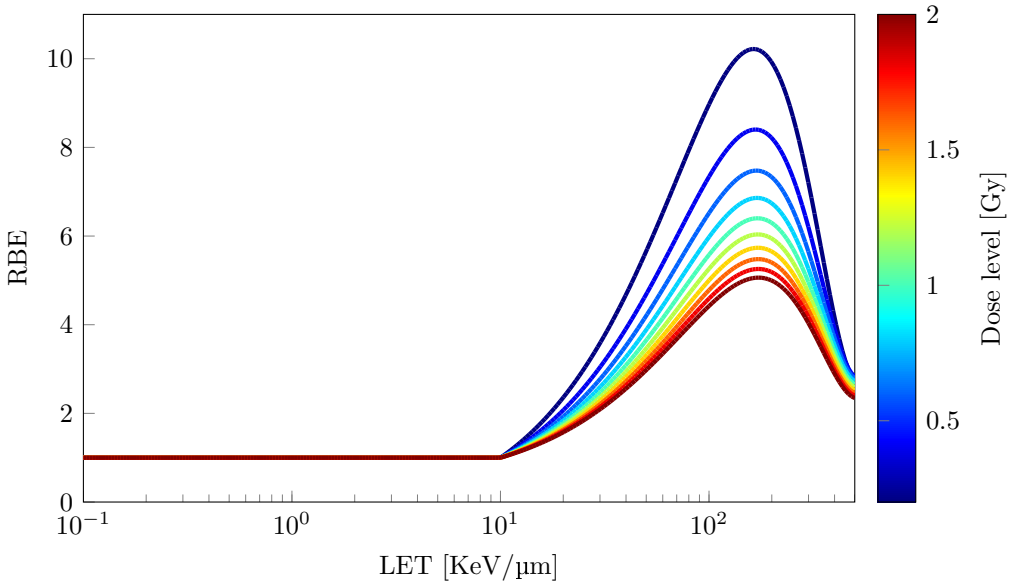

Figure 6.6: RBE as function of LET and dose. The function har been set to 1 between 0.1 and 10 KeV/µm. 4 order polynomial fit has been made between 10 and 1000 KeV/µm, with a constraint to RBE = 1 at 10 KeV/µm. The BWF is limited to the relevant area between 0.1 and 500 KeV/µm. The dose dependency is in principle continuous, however only the discrete lines for every 0.2 Gy between 0.2 and 2 Gy are shown here.

A large portion of the LET spectra from a proton beam is in the region below 10 KeV/µm and almost all values in the LET_d distribution are below this value, as seen in figure 6.1. The effect of correcting the BWF can be seen in figure 6.7. The physical dose and the $BED_{1.1}$ are as in figure 6.4, but the BED values calculated by the corrected BWF is lower at allmost all positions. The $RBE_{spectrum}$ is rising along with the depth. In the monoenergetic example in figure 6.7 A, the $RBE_{spectrum}$ is almost 1.18 at the maximum of the Bragg peak. In example B in figure 6.7, the $RBE_{spectrum}$ reaches a top of around 1.17 at the end of the SOBP. The $RBE_{average}$ is almost 1 at all depths, thus the $BED_{average}$ follows the physical dose distribution at all positions, besides in the region of the distal dose falloff. The $RBE_{average}$ rises up to 1.4 at the end of the distal dose falloff, but the

physical dose is only 0.6 Gy here, therefore the $\mathrm{BED}_{average}$ only becomes 0.85, still below to $\mathrm{BED}_{spectrum}$.

The ratio $\mathrm{BED}_{spectrum}/\mathrm{BED}_{average}$ follow more or less the $\mathrm{RBE}_{spectrum}$ distrubution, as the $\mathrm{RBE}_{average}$ is almost 1 at all positions. The ratio peaks at the distal end of the bragg beak, reaching 117%.

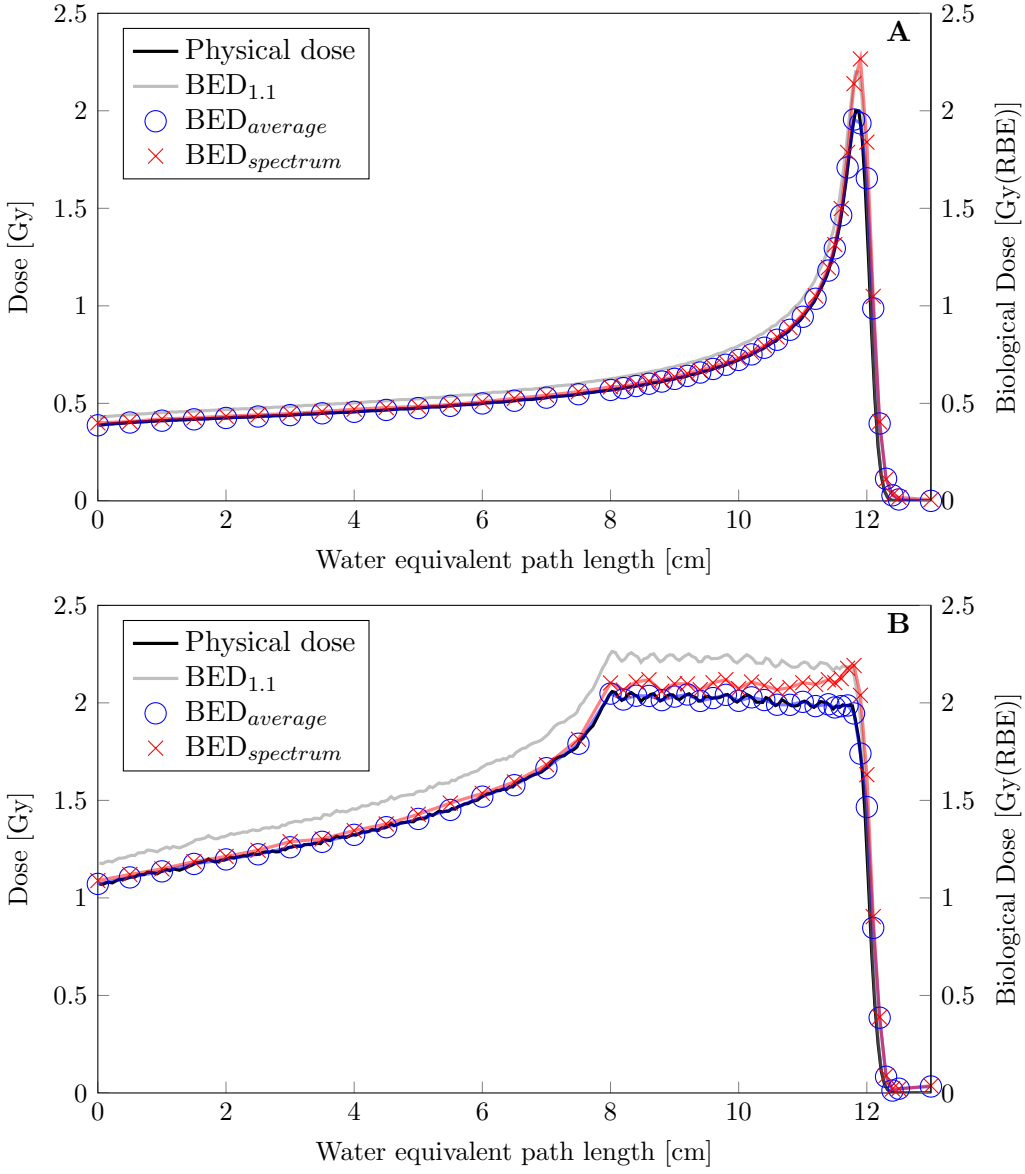

Figure 6.7: The depth dose curves of the proton setups. The BEDs are based on the dog leg fitted BWF, as shown in figure 6.6. The BED of a constant RBE of 1.1 is also plotted for comparison. **A:** The monoenergetic setup. **B:** The SOBP setup.

Chapter 7

Discussion

7.1 The spectrum method vs. the average method

The present work was performed in order to investigate whether the two methods yield significantly different results. The analysis is done individually for the different protons and carbon ions.

7.1.1 General analytical solution

By inserting 5.2 into equation 5.1 and 5.3, we achieve:

$$\mathrm{RBE}_{spectrum} = \int_0^\infty a_0 + a_1 L + a_2 L^2 + a_3 L^3 + a_4 L^4 d(L)\mathrm{d}L \tag{7.1}$$

$$\mathrm{RBE}_{spectrum} = a_0 \underbrace{\int_0^\infty d(L)\mathrm{d}L}_{=1} + a_1 \underbrace{\int_0^\infty L d(L)\mathrm{d}L}_{=\mathrm{LET}_d} + \tag{7.2}$$

$$a_2 \int_0^\infty L^2 d(L)\mathrm{d}L + a_3 \int_0^\infty L^3 d(L)\mathrm{d}L + a_4 \int_0^\infty L^4 d(L)\mathrm{d}L \tag{7.3}$$

$$\mathrm{RBE}_{spectrum} = a_0 + a_1 \mathrm{LET}_d + a_2 \int_0^\infty L^2 d(L)\mathrm{d}L + a_3 \int_0^\infty L^3 d(L)\mathrm{d}L + a_4 \int_0^\infty L^4 d(L)\mathrm{d}L, \tag{7.4}$$

where the two first terms are solved by inserting equation 3.4 and 3.17. And by writing out the average calculation method we get:

$$\mathrm{RBE}_{average} = a_0 + a_1 \mathrm{LET}_d + a_2 \mathrm{LET}_d + a_3 \mathrm{LET}_d + a_4 \mathrm{LET}_d. \tag{7.5}$$

As marked, the two first terms are the same. The two calculation methods only differ from the last three terms. This property is used in the further discussion.

7.1.2 Proton beams

Full fit

As the differences in the calculated BED is maximum 2% along the SOBP and 5% in the small area of the distal dose falloff, the BED is more or less independent of the calculation method. This difference is not seen as significant, as a potential dose error of 2 % would still satisfy the prescriptions limits given by ICRU [25], as mention in section 2.4.3. Also, the uncertainty in the cellular data and the fitting of the BWF to these data poses could potentially yield a uncertainty in the biological dose, as discussed later.

A constant RBE of 1.1 for protons is still used in clinics. The results show that the tumour volume still get at least the prescribed dose. This is considered as good, as the 1.1 value is set to a conservative level.

The maximum LET value in the LET spectra from a proton beam is about 50-60 KeV/µm, as noted in section 6.1. The effective LET region of interest for protons is then between 0.1 and 60 KeV/µm. If we analyse the BWF curves from figure 6.3 at this region, a close to linear relationship between LET and RBE is found. The more or less linear relationship for this region is also noted by Paganetti [14, 6]. If we assume that the BWF is linear, we could rewrite the fourth order polynomial in equation 5.2 to a first order polynomial:

$$r(L) = a_0 + a_1 L. \tag{7.6}$$

By utilizing a linear BWF, we would then gain the trivial analytical solution:

$$\mathrm{RBE}_{average} = \mathrm{RBE}_{spectrum} = a_0 + a_1 \mathrm{LET}_d. \tag{7.7}$$

The equality between $\mathrm{RBE}_{average}$ and $\mathrm{RBE}_{spectrum}$ can be seen in figure 6.4 as the circles and crosses align near perfectly. As long as we assume a linear relationship, there is no need to calculate by the spectrum method. As noted by Grassberger and Paganetti [11], the average method is more practical to implement. Furthermore the principle of a single quantity LET_d is probably simpler to grasp and understand, than a full spectrum. Thus, for protons with a linear BWF, the average method can therefore be recommended.

Dog leg Fit

When the BWF is no longer linear in the LET region of interest, the two different estimates will not be identical, as shown in figure 6.7 for the "dog leg fit" BWF. For both the pristine Bragg peak example and the SOBP example, the LET_d is below 10 KeV/µm at almost all measured positions. The RBE value of the average method is 1 at all of these positions. However, the spectra at these positions exceeds up to almost 60 KeV/µm, where the $r(L)$ is steep. The RBE is then increasing along towards the distal end of the SOBP. There is a non negligible difference between the estimates in this example. This nonlinear BWF was included to indicate that the two calculation methods could give two different estimates. The limit at 10 KeV/µm is arbitrary chosen, to show that a dog legged BWF might disfavour the average method. The BWF used in this example might be a bit extreme, but it illustrates the potential significance of selection of the calculation methods. Depending of the value of the dog leg around 10 KeV/µm, the BWF might be too nonlinear and the spectrum method could be most appropriate method to use.

7.1.3 Carbon ion beams

From equation 7.4 and 7.5, we can see that the two different calculation methods only differs from the last three terms. In practice this means that the methods give different results when the LET spectrum is covering a broad area where three last terms have impact. As a_3, a_4 and a_5 are relatively small compared to a_1 and a_2, this only happens at high LET value. This effect is observed in particular for carbon ions in the proximal and mid SOBP, as seen in figure 6.5 B. The beam then consists of carbon ions both low and high energy, with high and low LET value. This wide spectrum then covers the area around the peak in the BWF with a LET_d with around 60 KeV/µm, as seen in figure 6.2. At 2 Gy, this corresponds to RBE of 3.2, when calculated with the average method.

By calculating with the spectrum method, the low energetic carbon ions have LET values far above 200 KeV/µm, above the optimal LET value for cell killing. The high energetic ions have low LET value, also implying a low RBE. When calculated together, the spectrum method only gets an effective RBE of about

2.7. If the dosimetric constrains issued by ICRU, covered in section 2.4.3, should be followed, this calculation difference is significant, and should not be neglected.

Even though phenomenological LET based models are not regarded as applicable for carbon ion therapy [9], the averaging issue should still be regarded for other models. The old dose algorithm used at NIRS had the same averaging fault, and is partly the reason why NIRS recently transferred to a new dose calculation model[48].

7.2 Assumptions in RBE model

As seen in the scatter plots in figure 4.4, the vertical spread between the different datapoints is great. In our model, the best fitted polynomial is fitted to plots like this. This answer thus then only offer us the most general answer. The uncertainty of this answer is high. In this thesis, the uncertainty has not been calculated. This is a complicated quantity, dependent on the uncertainty from the cell experiments, the selection and fitting of a representative BWF to the data as well as the uncertainty in data simulations. The remarkable spread and estimation of uncertainty from the experimental data is also noted by Paganetti [14]. Uncertainties is important to incorporate in RBE models, as a the whole tumour should receive the prescribed dose. A high uncertainty would reduce the tumor control probability (TCP) and increase the NTCP.

It is therefore desired to decrease the uncertainty. This can be done by optimizing the RBE model. Some of the short comings of the model is discussed in the following section.

7.2.1 A monoenergitical database?

The databases includes the LET_d of the particle, but does not describe the spectrum $d(L)$ the cells were irradiated with. Hence, the BWF is a function dependent on LET_d. The average method should then be the most logical and correct method for BED calculation, as also LET_d is used as input parameter. The spectrum method depends on a BWF where every LET value corresponds to the biological effect of that specific LET value. To create a more accurate BWF like that, the LET spectrum needs to be logged when the cells are irradiated. Regression

fitting to a scatter plot will not be the best optimal way to find the BWF. An unfolding code could analyse the effect of several LET spectra and be able to find the natural BWF. The code should read $d(L)$ and the RBE, and find $r(L)$ by optimizing equation 5.1. A similar approach was used to find a BWF for lineal energy [68, 53].

Otherwise, we could assume that the $d(L)$ of all experiments is like a Dirac delta function with $d(L) = \delta(L - \text{LET}_d)$. This implies that RBE(L) = $r(L)$ = $r(\text{LET}_d)$. This assumption was used, and is the reason why the same BWF was used for both calculations.

A broad SOBP LET spectrum and a narrow monoenergetic spectrum, both with the same LET_d, are shown in figure 7.1. If we assume that the BWF drawn in the figure is the "true" BWF, we could then calculate the RBE from both spectra with equation 5.1. For this example, an RBE of 1 and 1.13 is achieved, for the monoenergitical and the SOBP spectra, respectively. This effect will increase the vertical spread in LET-RBE plots, as the ones in figure 4.4.

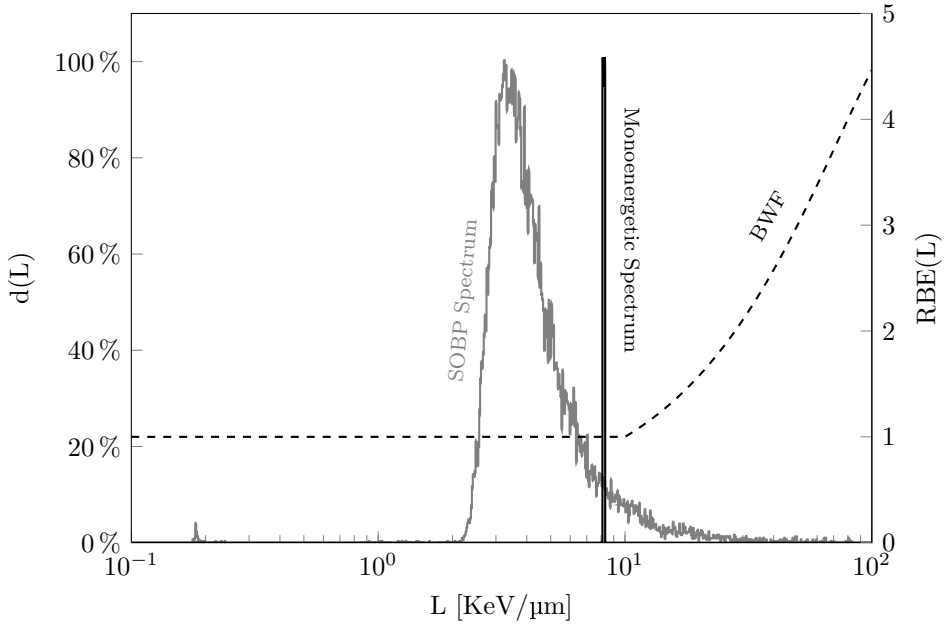

Figure 7.1: An example of how two different spectrum of a proton beam with the same LET_d, will give a different RBE. Both the SOBP spectrum and theoretical monoenergitical spectrum have been renormalized, such that the left axis shows the relative intensity of every LET value L, against the maximum LET value. The LET_d is 8.22 KeV/µm for both spectra. The dashed line show a possible BWF, with a constant RBE of 1 below 10 KeV/µm.

If all experiments were done with monoenergitical beams, the spread in RBE values would then be less. Such experiments could only be done in vitro, as the beam needs to be pristine as it reaches it target. This database would be suitable to create a BWF for the spectrum method. And if the uncertainty in the potential new database is lower, it is therefore hypothesized that the spectrum method will give a more accurate biological dose compared to the average method.

7.2.2 Environment dependence

The database compiled by Paganetti consists of different experiments [14]. Most of them are done in vitro, however a few are in vivo. In general, the biological effect is higher for cells irradiated in vitro [69]. This is shown in an article from 2002, where it is concluded that protons have a constant RBE of approximately 1.2 for cells in vitro, compared to 1.1 for cells in vivo. An analysis based on separation of in vivo and in vitro experiments may shed additional light over the issues investigated in this work.

The dose calculation algorithm from NIRS uses two different definitions of BED [48]. D_{bio} is the biological dose calculated from the in vitro cell lines, while D_{clinical} is the BED when the same physical dose is given to a patient. The clinical BED is found by a calibrated constant scalar named F_{NIRS}. We then have:

$$D_{\text{clinical}} = D_{\text{bio}} \times F_{\text{NIRS}}. \tag{7.8}$$

A similar approach could be used to further explore the topic of this thesis, even if the database is exclusively based upon in vitro experiments.

7.2.3 Particle dependence

The model also assumes that there is no significant dependence on the particle type, as concluded by Sørensen et al [66]. But this statement is disputed by others [70]. It has previously been shown that the peak in the LET-RBE relationship is shifted towards higher LET value for heavier ions, as shown in figure 7.2 [71]. In practice, this means that protons would have a higher RBE at lower LET values. This adjustment could enlarge the BED for the proton beams in figure 6.4 and 6.7.

If this effect was well quantified, it could be incorporated into the model designed in this work. It is possible to divide the major LET spectrum into minor LET spectra for every particle passing every measurement point. We would then have a LET spectrum $d_i(L)$ for ion number i with the corresponding $r_i(L)$. This would then result in several RBE_i. The weighting of the different RBE values could be done by the deposited dose by the particle type, the D_i.

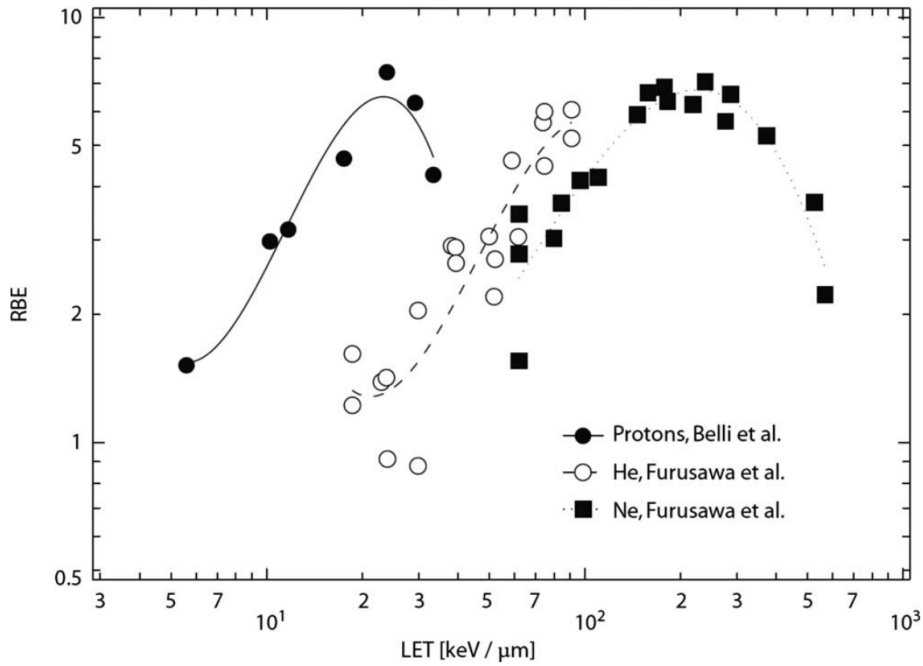

Figure 7.2: The relationship between LET and $\mathrm{RBE}_\alpha = \alpha_{ion}/\alpha$ for three different ion types. Redrawn by Scholz [71] with data from Belli et al. [45] and Furusawa et al. [47].

The particle dependency in the LET-RBE relationship is partly why the lineal energy y is preferred over LET. Microdosimetric spectra consist of the deposited energy in the microscopic volume, independent of the type of particle [53]. Microdosimetric models, like the microdosimetric kinetic model (MKM), use this ion independent property to predict the RBE. A version of the MKM is newly introduced as the new biological dose calculation algorithm for carbon ion therapy at NIRS [48].

7.2.4 Cell dependence

In the model made in this work, no tissue differentiation is made. This is similiar to model used at NIRS, also for the new system. However, as shown in figure 7.3, the internal variation between the cell types is large. This could be quantified by the α/β ratio. Some radiobiological models, as LEM and Wedenbergs model, are includes the tissue dependency [35] [51]. Paganetti also discusses the possibility to adjust the constant RBE of 1.1 for protons to 1.2 for fast reacting tissue with an α/β ratio below 3 Gy [6].

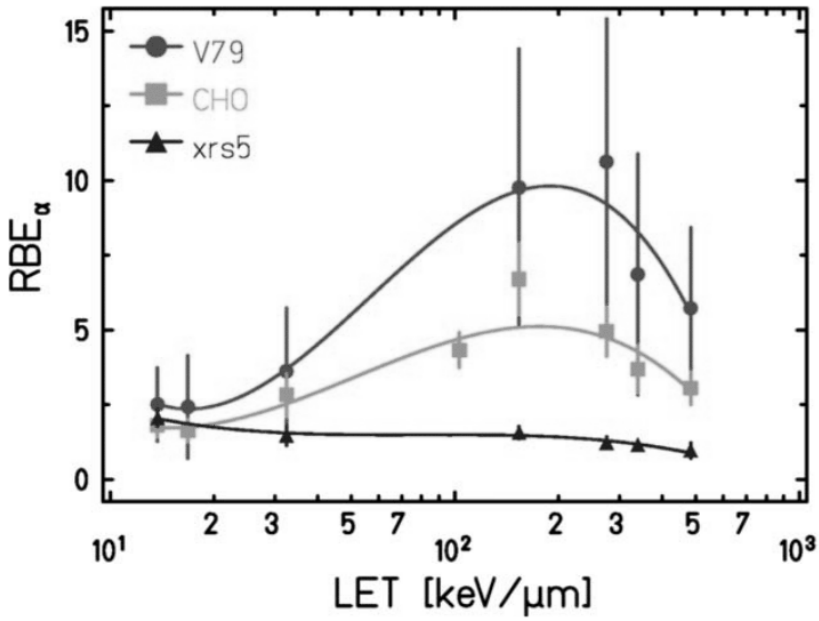

Figure 7.3: The $\text{RBE}_\alpha = \alpha_{ion}/\alpha$ function of LET for three different cell lines in vitro. Made by Weyrahter [72].

Our BWF could be group into multiple tissue dependent BWFs. This could be done by only fitting the polynomial to different intervals of α/β ratio, similar to what Paganetti did in his review article [14]. By making a BWF for every particle and tissue type, the number of cell experiments needed multiplies quickly. This is a complicated and time consuming process, as noted by Scholz et al [73]. The massive need for experimental data is one of the major disadvantages for the pure phenomenological models, compared to the analytical models such as the LEM.

7.2.5 Validity of the LQ model at low doses

While the LQ-model introduces a simple relation between the dose and effect on cell survival, the model breaks down for doses below 1 Gy for some cell lines [74]. This is due to a phenomenon termed low dose hyper-radiosensitivity (HRS), where the cells initially are extra sensitive to the radiation dose until approximately 10 cGy is given. But when transferring to higher doses, the cells slightly become more radioresistant. This region of increased radioresistance (IRR) is commonly found between 20 and 80 cGy. It is not yet known why this effect occurs, but it might be linked to asynchronous cell cycle distribution, an increased DNA repair capability in this region, or other radiation hormesis effects.

At the moment, the assumption that the LQ also holds for low doses still need to used. For radiation given in 2 Gy fractions, the problem is minimal, since the full SOBP is approximately 2 Gy and the entrance plateau is normally above 1 Gy. But the HRS could make a difference in the low dose regions of the depth dose curve, typically at the end of the distal dose falloff. For carbons and other ions, the fraction tail is also a low dose region where the HRS effect could make an impact. And also in plans utilizing multiple fields for every fraction.

7.3 Suggestions for further work

If all assumptions holds, the spectrum method should in theory estimate a more accurate answer than the average method. The spectrum method is the most comprehensive and includes as much information as possible before it deduces a single RBE value. And the result show that introducing the full LET spectrum in radiobiological models does make a significant impact on the estimated dose, as long as a non linear BWF is assumed. It is recommended to test both methods by benchmarking the answers against experimental RBE values or analytical radiobiological models, as the LEM [35].

At the moment, the model is basic and general. As written in the last section, many of assumptions used are loosely based. But the model could differentiated to be dependent on tissue type and particle type, as described. The effect of the different dependencies could then be investigated, as done by others [66]. I predict that a differentiated model will give a more accurate estimation of the dose.

Even though an RBE of 1.1 is still used for protons in clinics, this might change to a model based RBE, as for carbon ions [6]. Calculating with a RBE of 1.1 still delivers enough dose to the tumour, even if a variable RBE in reality is present, as shown in figure 6.4. Planning with a constant or a variable RBE would then have little impact on the TCP. However, the biological dose to other organs at risk (OAR) nearby could be underestimated with a constant RBE. Specially at the distal edge, where the LET_d is high. The potential extra OAR dose could be implemented into NTCP models, and comparison studies could be done [75].

In this work, only four examples have been simulated, with only protons and carbon. All of the simulations was based on a single field in a water phantom. However, the principle of using a $d(L)$ dependent RBE model should also hold for other particles like helium and oxygen, and for other setups. The target could also be exchanged. Potentially, the methodology should be possible to use on DICOM-images, to investigate the effect inside human tissue [76]. Monte Carlo simulation tools like FLUKA or TOPAS are able to implement DICOM images in their geometry setup and score LET spectrum [57, 58, 77]. Other clinical treatment planning software (TPS) like Raystation is able to score LET_d, and possible also the LET spectrum [78].

The investigation of multiple fields is particular interesting. With using two treatment fields or more, it is possible to optimize not only for the physical dose, but also for the cell survival or LET_d [79, 60]. Optimization with respect to the single scalar LET_d is feasible, but it is not possible to optimize to the LET spectrum directly. Instead it should be possible to optimize to the RBE or BED, calculated by the spectrum method.

LET optimization and LET painting is of special interest for treatment of hypoxic cells. Experiments have shown that hypoxic cells are more responsive to high LET particles [80]. This could be quantified by the LET dependent oxygen enhancement ratio (OER). Most OER models today relate to LET_d. These models could potentially be connected to the LET spectrum instead, in the same matter as the RBE model used in this thesis.

The replacement of the average LET value by the LET spectrum could also be used in other radiobiological models.

Chapter 8

Conclusion

The effect of changing the input parameter in a LET dependent radiobiological model has been investigated. Two different methods for calculating the RBE and BED of proton and carbon ion beams was used. Models based on the LET_d has been prevalent. However, by utilizing the full dose weighted LET spectrum, more information on the radiation quality of the beam could be used in the estimation of the biological dose.

The results in this work indicate that the BED based on the full LET spectra differ from BED calculated by use of LET_d with less than 2% in most positions in proton therapy, as long as the relationship between LET and RBE is assumed to be close to linear. For both models, the RBE is above the clinical used RBE of 1.1, and increasing along the SOBP. The differences in carbon ion therapy is however much more significant, especially along the SOBP covering the tumour volume. The two methods could differ up to 17%. The possible calculation fault by averaging the LET spectrum, could make purely LET_d based models less trustworthy.

Yet, there are several limitations in the approach of this work, and only a simple comparison has been done. Benchmarking against other models or experiments is recommended. The model used is also highly general, and could be further differentiated. The concept of utilizing the LET spectrum instead of the average LET should be investigated further, as it could make a impact in some radiobiological models.

Appendix A

FLUKA Monte Carlo Script

```
     *$ CREATE SOURCE.FOR
*COPY SOURCE
*
*=== source ============================================================*
*
      SUBROUTINE SOURCE ( NOMORE )

      INCLUDE '(DBLPRC)'
      INCLUDE '(DIMPAR)'
      INCLUDE '(IOUNIT)'
*
*----------------------------------------------------------------------*
*                                                                      *
*     Copyright (C) 1990-2006      by    Alfredo Ferrari & Paola Sala  *
*     All Rights Reserved.                                             *
*                                                                      *
*                                                                      *
*     New source for FLUKA9x-FLUKA200x:                                *
*                                                                      *
*     Created on 07 january 1990   by    Alfredo Ferrari & Paola Sala  *
*                                                Infn - Milan          *
*                                                                      *
*     Last change on 03-mar-06     by    Alfredo Ferrari               *
*                                                                      *
*  This is just an example of a possible user written source routine.  *
```

```
*  note that the beam card still has some meaning - in the scoring the *
*  maximum momentum used in deciding the binning is taken from the     *
*  beam momentum.  Other beam card parameters are obsolete.            *
*                                                                      *
*----------------------------------------------------------------------*
*
      INCLUDE '(BEAMCM)'
      INCLUDE '(FHEAVY)'
      INCLUDE '(FLKSTK)'
      INCLUDE '(IOIOCM)'
      INCLUDE '(LTCLCM)'
      INCLUDE '(PAPROP)'
      INCLUDE '(SOURCM)'
      INCLUDE '(SUMCOU)'
*
      INCLUDE '(CASLIM)'
*
c $FLUPRO/flutil/ldpm3qmd source_SAM.f -o flukadpm3_sam
      DOUBLE PRECISION ENERGY(65000), XPOS(65000), YPOS(65000)
      DOUBLE PRECISION FWHM(65000), PART(65000)
      INTEGER NWEIGHT


      SAVE ENERGY, XPOS, YPOS
      SAVE FWHM, PART
      SAVE NWEIGHT


      LOGICAL LFIRST
*
      SAVE LFIRST
      DATA LFIRST / .TRUE. /
*======================================================================*
*                                                                      *
*                 BASIC VERSION                                        *
*                                                                      *
*======================================================================*
      NOMORE = 0
*  +-------------------------------------------------------------------*
*  |  First call initializations:
      IF ( LFIRST ) THEN
```

```
*  |  *** The following 3 cards are mandatory ***
     WRITE(LUNOUT,*) ' NB SOURCE_SAM4 INVOKED'
          TKESUM = ZERZER
          LFIRST = .FALSE.
          LUSSRC = .TRUE.

ccc only absolute path or
          OPEN(44, FILE = '../sobp.dat',
     $         STATUS = 'OLD')
          WRITE(LUNOUT,*) 'NB SOURCE ZPOS fixed to', ZBEAM



          NWEIGHT = 0
          WSUM = 0.0
          DO
*  fortran arrays start with 1
             NWEIGHT = NWEIGHT + 1
             IF (NWEIGHT .GT. 65000) THEN
                WRITE(LUNOUT,*) 'NB SOURCE ERROR: too many beamlets'
             ENDIF

             READ (44, 3, END=10 ) ENERGY(NWEIGHT),
     $            XPOS(NWEIGHT), YPOS(NWEIGHT),
     $            FWHM(NWEIGHT), PART(NWEIGHT)
 3           FORMAT(F10.4,F10.4,F10.4,F10.4,E10.4)
             WSUM = WSUM + PART(NWEIGHT)
             ENERGY(NWEIGHT) = ENERGY(NWEIGHT)
          ENDDO
 10       CONTINUE
*         fix index
     NWEIGHT = NWEIGHT - 1
          WRITE(LUNOUT,*) 'NB SOURCE beamlets found:', NWEIGHT
          WRITE(LUNOUT,*) 'NB SOURCE Particle sum (float) :', WSUM
          WRITE(LUNOUT,*) 'NB SOURCE TODO: particle sum is not exact.'

* check for gaussian, for future implementation
          IF ((Ldygss) .AND. (Ldxgss)) THEN
             WRITE(LUNOUT,*) 'NB SOURCE GAUSSIAN: TRUE'
          ELSE
             WRITE(LUNOUT,*) 'NB SOURCE GAUSSIAN: FALSE'
          ENDIF
```

```
      END IF

*** Sample a beamlet ****************************

      RAN = FLRNDM(111)

*     http://infohost.nmt.edu/tcc/help/lang/fortran/scaling.html
*     If you want an integer between i and j inclusive
*     use int(rand(0)*(j+1-i))+i
*     i hope hope FLRNDM [0,1[ ??
      NRAN = INT(RAN * NWEIGHT) + 1

*     If you want a real number in the interval [x,y),
*      use this expression:
*     (rand(0)*(y-x))+x

      IF ((NRAN .GT. NWEIGHT) .OR. (NRAN .LT. 1)) THEN
         WRITE(LUNOUT,*) 'NB SOURCE BOUND ERROR. NRAN, RAN:', NRAN, RAN
      END IF

      ENK = ENERGY(NRAN)
      XBEAM = XPOS(NRAN)
      YBEAM = YPOS(NRAN)
      XSPOT = FWHM(NRAN)/2.35482
      YSPOT = XSPOT

*      WRITE(LUNOUT,*) 'NB SOURCE SAM:', RAN,NRAN, ENK, XBEAM, YBEAM
*      WRITE(LUNOUT,*) 'NB SOURCE SAM2:', XSPOT,YSPOT, PART(NRAN)

*** End of beamlet sample ************************************************




*  +-------------------------------------------------------------------*
*  Push one source particle to the stack. Note that you could as well
*  push many but this way we reserve a maximum amount of space in the
*  stack for the secondaries to be generated
```

```
* Npflka is the stack counter: of course any time source is called it
* must be =0
      NPFLKA = NPFLKA + 1
* Wt is the weight of the particle
**       WTFLK  (NPFLKA) = ONEONE          set new weight
      WTFLK  (NPFLKA) = PART(NRAN)
      WEIPRI = WEIPRI + WTFLK (NPFLKA)
* Particle type (1=proton.....). Ijbeam is the type set by the BEAM
* card
*  +-------------------------------------------------------------------*
*  |  (Radioactive) isotope:
      IF ( IJBEAM .EQ. -2 .AND. LRDBEA ) THEN
         IARES  = IPROA
         IZRES  = IPROZ
         IISRES = IPROM
         CALL STISBM ( IARES, IZRES, IISRES )
         IJHION = IPROZ  * 1000 + IPROA
         IJHION = IJHION * 100 + KXHEAV
         IONID  = IJHION
         CALL DCDION ( IONID )
         CALL SETION ( IONID )
*  |
*  +-------------------------------------------------------------------*
*  |  Heavy ion:
      ELSE IF ( IJBEAM .EQ. -2 ) THEN
         IJHION = IPROZ  * 1000 + IPROA
         IJHION = IJHION * 100 + KXHEAV
         IONID  = IJHION
         CALL DCDION ( IONID )
         CALL SETION ( IONID )
         ILOFLK (NPFLKA) = IJHION
*  |  Flag this is prompt radiation
         LRADDC (NPFLKA) = .FALSE.
*  |
*  +-------------------------------------------------------------------*
*  |  Normal hadron:
      ELSE
         IONID = IJBEAM
         ILOFLK (NPFLKA) = IJBEAM
*  |  Flag this is prompt radiation
         LRADDC (NPFLKA) = .FALSE.
```

```
      END IF
*  |
*  +-------------------------------------------------------------------*
* From this point .....
* Particle generation (1 for primaries)
      LOFLK  (NPFLKA) = 1
* User dependent flag:
      LOUSE  (NPFLKA) = 0
* User dependent spare variables:
      DO 100 ISPR = 1, MKBMX1
         SPAREK (ISPR,NPFLKA) = ZERZER
 100  CONTINUE
* User dependent spare flags:
      DO 200 ISPR = 1, MKBMX2
         ISPARK (ISPR,NPFLKA) = 0
 200  CONTINUE
* Save the track number of the stack particle:
      ISPARK (MKBMX2,NPFLKA) = NPFLKA
      NPARMA = NPARMA + 1
      NUMPAR (NPFLKA) = NPARMA
      NEVENT (NPFLKA) = 0
      DFNEAR (NPFLKA) = +ZERZER
* ... to this point: don't change anything
* Particle age (s)
      AGESTK (NPFLKA) = +ZERZER
      AKNSHR (NPFLKA) = -TWOTWO
* Group number for "low" energy neutrons, set to 0 anyway
      IGROUP (NPFLKA) = 0
*********************************************************************

*sample a gaussian position
*      IF (Ldygss) THEN
      CALL FLNRR2 (RGAUS1, RGAUS2)
      XFLK   (NPFLKA) = XBEAM + XSPOT * RGAUS1
      YFLK   (NPFLKA) = YBEAM + YSPOT * RGAUS2
      ZFLK   (NPFLKA) = ZBEAM

*      WRITE(LUNOUT,*) 'NB SOURCE gaussian sampled'

* Cosines (tx,ty,tz) (fix along z axis)
```

```
      TXFLK  (NPFLKA) = ZERZER
      TYFLK  (NPFLKA) = ZERZER
      TZFLK  (NPFLKA) = ONEONE
*      WRITE(LUNOUT,*) 'NB SOURCE cosines set'
*********************************************************************
* Particle momentum
*      PMOFLK (NPFLKA) = PBEAM
*      WRITE(LUNOUT,*) 'NB SOURCE mark',AM (IONID)
       CALL FLNRRN(RGAUSS)
       PMOFLK (NPFLKA) = SQRT ( ENK* ( ENK
     &     + TWOTWO * AM (IONID) ))
     &     +DPBEAM*RGAUSS/2.35482


* Kinetic energy of the particle (GeV)
* set energy
      TKEFLK (NPFLKA) = SQRT(PMOFLK(NPFLKA)**2 + AM(IONID)**2)
     &      -AM(IONID)

*      WRITE(LUNOUT,*) 'NB SOURCE set ekin'


* Polarization cosines:
      TXPOL  (NPFLKA) = -TWOTWO
      TYPOL  (NPFLKA) = +ZERZER
      TZPOL  (NPFLKA) = +ZERZER
*      WRITE(LUNOUT,*) 'NB SOURCE pol set'
*+++++++++++++++++++++++++++++++++++++++++++++++++++++++++++++++++++++
*+++++++++++++++++++++++++++++++++++++++++++++++++++++++++++++++++++++
*  Calculate the total kinetic energy of the primaries: don't change
      IF ( ILOFLK (NPFLKA) .EQ. -2 .OR. ILOFLK (NPFLKA) .GT. 100000 )
     &   THEN
         TKESUM = TKESUM + TKEFLK (NPFLKA) * WTFLK (NPFLKA)
      ELSE IF ( ILOFLK (NPFLKA) .NE. 0 ) THEN
         TKESUM = TKESUM + ( TKEFLK (NPFLKA) + AMDISC (ILOFLK(NPFLKA)) )
     &          * WTFLK (NPFLKA)
      ELSE
         TKESUM = TKESUM + TKEFLK (NPFLKA) * WTFLK (NPFLKA)
      END IF
      RADDLY (NPFLKA) = ZERZER
```

```
*      WRITE(LUNOUT,*) 'NB SOURCE mark'

*  Here we ask for the region number of the hitting point.
*     NREG (NPFLKA) = ...
*  The following line makes the starting region search much more
*  robust if particles are starting very close to a boundary:
       CALL GEOCRS ( TXFLK (NPFLKA), TYFLK (NPFLKA), TZFLK (NPFLKA) )
       CALL GEOREG ( XFLK  (NPFLKA), YFLK  (NPFLKA), ZFLK  (NPFLKA),
     &               NRGFLK(NPFLKA), IDISC )
*      WRITE(LUNOUT,*) 'NB SOURCE mark2'
*  Do not change these cards:
       CALL GEOHSM ( NHSPNT (NPFLKA), 1, -11, MLATTC )
       NLATTC (NPFLKA) = MLATTC
       CMPATH (NPFLKA) = ZERZER
       CALL SOEVSV


*      WRITE(LUNOUT,*) 'NB SOURCE END'
       CLOSE(44)
       RETURN
*=== End of subroutine Source ======================================*
       END
```

Appendix B

MATLAB script

The script reads the position and dose data in the "dosedata" file. It also reads 50 "spectrumdata" files, each corresponding to a single position along the z-axis. The data is prosessed and written to "outputfile". The RBE values is calculated for every position by the function "RBEfromdatabases".

```
dosedata = load('filenamefordosefile.dat','-ascii');
doseposition = dosedata(:,1);
doseatposition = dosedata(:,4);

outputfile = fopen('filenameforoutputfile.dat','w');


binnumberoffirstscorer = 30;
positionoffirstscorer = 0.0;
binnumberoflastscorer = 79;

lastof1scorers = 46;
ekvidistanceof1scorers = 0.5;

lastof2scorers = 63;
ekvidistanceof2scorers = 0.2;

lastof3scorers = 74;
ekvidistanceof3scorers = 0.1;
```

```
lastof4scorers = 79;
ekvidistanceof4scorers = 0.5;

position = positionoffirstscorer;

for binnumber = binnumberoffirstscorer:binnumberoflastscorer
binnumber
position
if position == 0
    dose = doseatposition(1);
else
    for i = 1:length(doseposition)
    if doseposition(i) >= position
        dose = ((doseatposition(i)-doseatposition(i-1))/
        (doseposition(i)-doseposition(i-1))*
        ((position-doseposition(i-1)))+doseatposition(i-1);
    break
    end
    end
end
filenamestring  = sprintf('filenameLETspec_%d_tab.lis',binnumber);

spectrumdata = load(filenamestring,'-ascii');
value = spectrumdata(:,3);
startdistance = spectrumdata(:,1);
enddistance = spectrumdata(:,2);
meanbindistance = (enddistance+startdistance)/2;
bins = enddistance-startdistance;
errorpst = spectrumdataa(:,4)./100;

currentLETvalue = 0;
i = 1;

while currentLETvalue < 497
    weightedbins(i) = bins(i)*value(i);
    binslimited(i) = bins(i);
    valuelimited(i) = value(i);
    meanBDlimited(i) = meanbindistance(i);

    currentLETvalue = meanbindistance(i+1);
    i = i+1;
```

```
end
weightedsum = sum(weightedbins);

freqLETspectrum = valuelimited/weightedsum;
freqaverageLET = sum(meanBDlimited.*freqLETspectrum.*binslimited);

doseLETspectrum = meanBDlimited.*freqLETspectrum/freqaverageLET;
doseaverageLET= sum(meanBDlimited.*doseLETspectrum.*binslimited);

orderofpolynom = 4;
[RBEaverageLET RBEspectrum] = RBEfromdatabases(
    doseaverageLET, doseLETspectrum, binslimited, meanBDlimited,
    dose, orderofpolynom);

EffectivedoseAverageLET = dose*RBEaverageLET;
EffectivedoseLETspecter = dose*RBEspectrum;

RBEratio = RBEspectrum/RBEaverageLET;

fprintf(outputfile,'%0.4f    %0.4f    %0.4f    %0.4f    %0.4f
    %0.4f    %0.4f    %0.4f %0.4f\n', position, freqaverageLET,
    doseaverageLET, RBEaverageLET, RBEspectrum, RBEratio, dose,
    EffectivedoseAverageLET, EffectivedoseLETspecter);
if binnumber < lastof1scorers
    distance = ekvidistanceof1scorers;
elseif binnumber < lastof2scorers
    distance = ekvidistanceof2scorers;
elseif binnumber < lastof3scorers
    distance = ekvidistanceof3scorers;
elseif binnumber < lastof4scorers
    distance = ekvidistanceof4scorers;
end
position = position + distance;
end

fclose(outputfile);
```

The function "RBEfromdatabases" uses the LET_d and $d(L)$ as input, and outputs the $\text{RBE}_{spectrum}$ and $\text{RBE}_{average}$ quanities. The function loads the databases parameters, creates a scatter plot and fits a fourth order polynomial to it. The polynomial is then used as the BWF, to calculate $\text{RBE}_{spectrum}$ and $\text{RBE}_{average}$, which is returned to the main script. Also another similar function was made, to constraint the fit to start at 10 KeV/µm with a RBE value of 1.

```
function [RBEaverageLET RBEspectrum] = RBEfromdatabases(
    doseaverageLET, doseLETspectrum, binslimited, meanBDlimited,
    dose, orderofpolynom)

load PideandPaganettidatabase.mat

%Parameters:

%Databases
Pidedata=true;
Paganettidata=true;

%Ionchargelimit (only for PIDE):
chargelimitlow=0;
chargelimithigh=92;

%LET limit:
LETlimitlow=0.1;
LETlimithigh=1000;

%Alphabetaratio limit:
alphabetalimitlow=0;
alphabetalimithigh=220;

%Set vector coordinator:
n = 1;

%PIDEdatabase calculation:
if Pidedata==true
    for i = 1:length(alphaX_pide)
      %Alpha Beta ratio is not listed in the PIDE database:
```

```
      AlphaBetaRatioX = alphaX_pide(i)/betaX_pide(i);
      if (Charge_pide(i) >= chargelimitlow &&
      Charge_pide(i) <= chargelimithigh &&
      LET_pide(i) >= LETlimitlow && LET_pide(i) <= LETlimithigh &&
      AlphaBetaRatioX >= alphabetalimitlow &&
      AlphaBetaRatioX <= alphabetalimithigh)
        Survival = exp(-alphaX_pide(i)*dose-betaX_pide(i)*dose*dose);
        if betaI_pide(i) == 0;
        Iondose = -log(Survival)/alphaI_pide(i);
        else
        Iondose = (-alphaI_pide(i) +
        sqrt(alphaI_pide(i)^2-4*betaI_pide(i)*log(Survival))) /
        (2*betaI_pide(i));
        end
        RBE(n) = dose/Iondose;
        CorrespondingLETvalue(n) = LET_pide(i);
        n=n+1;
      end
    end
end

%Paganettidatabase calculation (The union datasets has been omitted
    from this database, but they exist in pide for charge = 1):
if Paganettidata==true
    for i = 1:length(alphaX_paganetti)
      %Alpha Beta ratio is not listed in the PIDE database:
      if (LET_paganetti(i) >= LETlimitlow &&
      LET_paganetti(i) <= LETlimithigh &&
      ratioX_paganetti(i) >= alphabetalimitlow &&
      ratioX_paganetti(i) <= alphabetalimithigh)
        Survival = exp(-alphaX_paganetti(i)
        *dose-betaX_paganetti(i)*dose*dose);
        if betaI_paganetti(i) == 0;
        Iondose = -log(Survival)/alphaI_paganetti(i);
        else
        Iondose = (-alphaI_paganetti(i) +
        sqrt(alphaI_paganetti(i)^2-4*betaI_paganetti(i)*log(Survival))) /
        (2*betaI_paganetti(i));
        end
        RBE(n) = dose/Iondose;
        CorrespondingLETvalue(n) = LET_paganetti(i);
```

```
            n=n+1;
        end
    end
end

rbefitparameters = polyfit(CorrespondingLETvalue,RBE,orderofpolynom)
RBEaverageLET = polyval(rbefitparameters,doseaverageLET);
bwf = polyval(rbefitparameters,meanBDlimited);
RBEspectrum = sum(doseLETspectrum.*binslimited.*bwf);

return
```

Bibliography

[1] Helse Vest v/Olav Mella et. al. Idefaserapport for etablering av protonterapisenter ved haukeland universitetssjukehus. 2014.

[2] T Bortfeld and R Jeraj. The physical basis and future of radiation therapy. *The British Journal of Radiology*, 84(1002):485–498, June 2011.

[3] Juliette Thariat, Jean-Michel Hannoun-Levi, Arthur Sun Myint, Te Vuong, and Jean-Pierre Gérard. Past, present, and future of radiotherapy for the benefit of patients. *Nature Reviews Clinical Oncology*, 10(1):52–60, January 2013.

[4] Herman Suit, Saveli Goldberg, Andrzej Niemierko, Alexei Trofimov, Judith Adams, Harald Paganetti, George T. Y. Chen, Thomas Bortfeld, Stanley Rosenthal, Jay Loeffler, and Thomas Delaney. Proton Beams to Replace Photon Beams in Radical Dose Treatments. *Acta Oncologica*, 42(8):800–808, January 2003.

[5] Helse Vest v/Olav Mella et. al. Planlegging av norsk senter for partikkelterapi. June 2013.

[6] Harald Paganetti. Relating Proton Treatments to Photon Treatments via the Relative Biological Effectiveness—Should We Revise Current Clinical Practice? *International Journal of Radiation Oncology • Biology • Physics*, 91(5):892–894, April 2015.

[7] G. Kraft. Tumor therapy with heavy charged particles. *Progress in Particle and Nuclear Physics*, 45, Supplement 2:S473–S544, 2000.

[8] Oliver Jäkel. Medical physics aspects of particle therapy. *Radiation Protection Dosimetry*, 137(1-2):156–166, November 2009.

[9] Harald Paganetti. The physics of proton biology. In *Proton Therapy Physics*. CRC Press, 2011.

[10] Lisa Polster, Jan Schuemann, Ilaria Rinaldi, Lucas Burigo, Aimee L. McNamara, Robert D. Stewart, Andrea Attili, David J. Carlson, Tatsuhiko Sato, José Ramos Méndez, Bruce Faddegon, Joseph Perl, and Harald Paganetti. Extension of TOPAS for the simulation of proton radiation effects considering molecular and cellular endpoints. *Physics in Medicine and Biology*, 60(13):5053, July 2015.

[11] C. Grassberger and H. Paganetti. Elevated LET components in clinical proton beams. *Physics in Medicine and Biology*, 56(20):6677, October 2011.

[12] Harald Paganetti. Range uncertainties in proton therapy and the role of Monte Carlo simulations. *Physics in Medicine and Biology*, 57(11):R99, June 2012.

[13] Thomas Friedrich, Uwe Scholz, Thilo ElsäSser, Marco Durante, and Michael Scholz. Systematic analysis of RBE and related quantities using a database of cell survival experiments with ion beam irradiation. *Journal of Radiation Research*, 54(3):494–514, May 2013.

[14] Harald Paganetti. Relative biological effectiveness (RBE) values for proton beam therapy. Variations as a function of biological endpoint, dose, and linear energy transfer. *Physics in Medicine and Biology*, 59(22):R419, November 2014.

[15] W. H. Bragg and R. Kleeman. LXXIV. On the ionization curves of radium. *Philosophical Magazine Series 6*, 8(48):726–738, 1904.

[16] W. H. Bragg and R. Kleeman. XXXIX. On the alpha particles of radium, and their loss of range in passing through various atoms and molecules. *Philosophical Magazine Series 6*, 10(57):318–340, September 1905.

[17] N. Bohr. II. On the theory of the decrease of velocity of moving electrified particles on passing through matter. *Philosophical Magazine Series 6*, 25(145):10–31, January 1913.

[18] H. Bethe and W. Heitler. On the Stopping of Fast Particles and on the Creation of Positive Electrons. *Proceedings of the Royal Society of London A: Mathematical, Physical and Engineering Sciences*, 146(856):83–112, August 1934.

[19] Bernard Gottschalk. Physics of Proton Interactions in Matter. In *Proton Therapy Physics*, Series in Medical Physics and Biomedical Engineering, pages 19–60. CRC Press, 2011.

[20] K. Gunzert-Marx, H. Iwase, D. Schardt, and R. S. Simon. Secondary beam fragments produced by 200 MeV u1 12c ions in water and their dose contributions in carbon ion radiotherapy. *New Journal of Physics*, 10(7):075003, July 2008.

[21] Thomas Bortfeld. An analytical approximation of the Bragg curve for therapeutic proton beams. *Medical Physics*, 24(12):2024–2033, December 1997.

[22] NIST US Department of Commerce. NIST Stopping-Power and Range Tables: Electrons, Protons, Helium Ions.

[23] S. Greilich, L. Grzanka, N. Bassler, C. E. Andersen, and O. Jäkel. Amorphous track models: A numerical comparison study. *Radiation Measurements*, 45(10):1406–1409, 2010.

[24] Ute Linz. Physical and Biological Rationale for Using Ions in Therapy. In Ute Linz, editor, *Ion Beam Therapy*, number 320 in Biological and Medical Physics, Biomedical Engineering, pages 45–59. Springer Berlin Heidelberg, 2012.

[25] *Prescribing, Recording, and Reporting Photon Beam Therapy.* Intl Commission on Radiation, Bethesda, Md, November 1993.

[26] Robert R. Wilson. Radiological use of fast protons. *Radiology*, 47(5):487–491, 1946.

[27] W. P. Levin, H. Kooy, J. S. Loeffler, and T. F. DeLaney. Proton beam therapy. *British Journal of Cancer*, 93(8):849–854, September 2005.

[28] Uli Weber and Gerhard Kraft. Design and construction of a ripple filter for a smoothed depth dose distribution in conformal particle therapy. *Physics in Medicine and Biology*, 44(11):2765, November 1999.

[29] Raymond E. Zirkle, Dorothy F. Marchbank, and Kathryn D. Kuck. Exponential and sigmoid survival curves resulting from alpha and X irradiation of aspergillus spores. *Journal of Cellular and Comparative Physiology*, 39(S1):75–85, March 1952.

[30] Leszek Grzanka. Modelling beam transport and biological effectiveness to develop treatment planning for ion beam radiotherapy. *arXiv:1410.1378 [physics]*, October 2014. arXiv: 1410.1378.

[31] *Linear Energy Transfer/Icru Report 16*. Intl Commission on Radiation, icru rpt16 edition edition, June 1970.

[32] F. Romano, G. a. P. Cirrone, G. Cuttone, F. Di Rosa, S. E. Mazzaglia, I. Petrovic, A. Ristic Fira, and A. Varisano. A Monte Carlo study for the calculation of the average linear energy transfer (LET) distributions for a clinical proton beam line and a radiobiological carbon ion beam line. *Physics in Medicine and Biology*, 59(12):2863, June 2014.

[33] Harald H. Rossi and Dr Marco Zaider. Microdosimetric Quantities and their Moments. In *Microdosimetry and Its Applications*, pages 17–27. Springer Berlin Heidelberg, 1996.

[34] Dieter Schardt, Thilo Elsässer, and Daniela Schulz-Ertner. Heavy-ion tumor therapy: Physical and radiobiological benefits. *Reviews of Modern Physics*, 82(1):383–425, February 2010.

[35] M. Scholz, A. M. Kellerer, W. Kraft-Weyrather, and G. Kraft. Computation of cell survival in heavy ion beams for therapy. *Radiation and Environmental Biophysics*, 36(1):59–66, March 1997.

[36] Jan J. Wilkens and Uwe Oelfke. Analytical linear energy transfer calculations for proton therapy. *Medical Physics*, 30(5):806–815, May 2003.

[37] Giovanna Martino. Microdosimetry measurements for c-12 pencil-like beams stopping in water, at gsi, darmstadt, germany. Master thesis, Universita Degli Studi Di Torino.

[38] Kenneth R. Kase, Bengt E. Bjärngard, and Frank H. Attix. *The Dosimetry of Ionizing Radiation*. Elsevier, October 2013.

[39] Eric J. Hall and Amato J. Giaccia. *Radiobiology for the Radiologist*. Lippincott Williams & Wilkins, 2006.

[40] Mark R. Kelley. *DNA Repair in Cancer Therapy: Molecular Targets and Clinical Applications*. Academic Press, 2012.

[41] Theodore T. Puck and Philip I. Marcus. Action of X-Rays on Mammalian Cells. *The Journal of Experimental Medicine*, 103(5):653–666, May 1956.

[42] Tohru Okada, Tadashi Kamada, Hiroshi Tsuji, Jun-etsu Mizoe, Masayuki Baba, Shingo Kato, Shigeru Yamada, Shinji Sugahara, Shigeo Yasuda, Naoyoshi Yamamoto, and others. Carbon ion radiotherapy: clinical experiences at National Institute of Radiological Science (NIRS). *Journal of radiation research*, 51(4):355–364, 2010.

[43] Christian P. Karger. Biological Models in Treatment Planning. In Wolfgang Schlegel, Thomas Bortfeld, and Anca-Ligia Grosu MD, editors, *New Technologies in Radiation Oncology*, Medical Radiology, pages 221–235. Springer Berlin Heidelberg, 2006.

[44] M. Krämer, W. K. Weyrather, and M. Scholz. The Increased Biological Effectiveness of Heavy Charged Particles: From Radiobiology to Treatment Planning. *Technology in Cancer Research & Treatment*, 2(5):427–436, October 2003.

[45] M. Belli F. Cera R. Cherubini M. Dalla Vecchia a. M. I. Haque F. Ianzini G. Moschini O. Sapora G. Simone M. a. Tabocchini P. Tiveron. RBE-LET relationships for cell inactivation and mutation induced by low energy protons

in V79 cells: further results at the LNL facility. *International Journal of Radiation Biology*, 74(4):501–509, January 1998.

[46] Mauro Belli, Daniela Bettega, Paola Calzolari, Roberto Cherubini, Giacomo Cuttone, Marco Durante, Giuseppe Esposito, Yoshiya Furusawa, Silvia Gerardi, Giancarlo Gialanella, Gianfranco Grossi, Lorenzo Manti, Renato Marchesini, Mariagabriella Pugliese, Paola Scampoli, Giustina Simone, Eugenio Sorrentino, Maria Antonella Tabocchini, and Lucia Tallone. Effectiveness of monoenergetic and spread-out bragg peak carbon-ions for inactivation of various normal and tumour human cell lines. *Journal of Radiation Research*, 49(6):597–607, November 2008.

[47] Y. Furusawa, K. Fukutsu, M. Aoki, H. Itsukaichi, K. Eguchi-Kasai, H. Ohara, F. Yatagai, T. Kanai, and K. Ando. Inactivation of Aerobic and Hypoxic Cells from Three Different Cell Lines by Accelerated 3he-, 12c- and 20ne-Ion Beams. *Radiation Research*, 154(5):485–496, November 2000.

[48] Taku Inaniwa, Nobuyuki Kanematsu, Naruhiro Matsufuji, Tatsuaki Kanai, Toshiyuki Shirai, Koji Noda, Hiroshi Tsuji, Tadashi Kamada, and Hirohiko Tsujii. Reformulation of a clinical-dose system for carbon-ion radiotherapy treatment planning at the National Institute of Radiological Sciences, Japan. *Physics in Medicine and Biology*, 60(8):3271, April 2015.

[49] J J Wilkens and U Oelfke. A phenomenological model for the relative biological effectiveness in therapeutic proton beams. *Physics in Medicine and Biology*, 49(13):2811–2825, July 2004.

[50] Alejandro Carabe, Maryam Moteabbed, Nicolas Depauw, Jan Schuemann, and Harald Paganetti. Range uncertainty in proton therapy due to variable biological effectiveness. *Physics in Medicine and Biology*, 57(5):1159, March 2012.

[51] Minna Wedenberg, Bengt K. Lind, and Björn Hårdemark. A model for the relative biological effectiveness of protons: The tissue specific parameter alpha/beta of photons is a predictor for the sensitivity to LET changes. *Acta Oncologica*, 52(3):580–588, August 2012.

[52] T. E. Blue, N. Gupta, and J. E. Woollard. A calculation of the energy dependence of the RBE of neutrons. *Physics in Medicine and Biology*, 38(12):1693, December 1993.

[53] T. Loncol, V. Cosgrove, J. M. Denis, J. Gueulette, A. Mazal, H. G. Menzel, P. Pihet, and R. Sabattier. Radiobiological Effectiveness of Radiation Beams with Broad LET Spectra: Microdosimetric Analysis Using Biological Weighting Functions. *Radiation Protection Dosimetry*, 52(1-4):347–352, April 1994.

[54] R. Gerlach, H. Roos, and A. M. Kellerer. Heavy Ion RBE and Microdosimetric Spectra. *Radiation Protection Dosimetry*, 99(1-4):413–418, June 2002.

[55] Harald Paganetti, Pawel Olko, Hubert Kobus, Regina Becker, Thomas Schmitz, Michael P. R. Waligorski, Detlef Filges, and Hans-Wilhelm Müller-Gärtner. Calculation of relative biological effectiveness for proton beams using biological weighting functions. *International Journal of Radiation Oncology*Biology*Physics*, 37(3):719–729, February 1997.

[56] Davide Moro. Experimental methods for microdosimetry, nanodosimetry and track structure determination: state of the art icon. In *3.rd ESTRO Forum*, 2015.

[57] A. Ferrari, P. R. Sala, A. Fasso, and J. Ranft. FLUKA: A Multi-Particle Transport Code. Technical report, Stanford Linear Accelerator Center (United States). Funding organisation: US Department of Energy (United States), 2005.

[58] T. T. Böhlen, F. Cerutti, M. P. W. Chin, A. Fassò, A. Ferrari, P. G. Ortega, A. Mairani, P. R. Sala, G. Smirnov, and V. Vlachoudis. The FLUKA Code: Developments and Challenges for High Energy and Medical Applications. *Nuclear Data Sheets*, 120:211–214, June 2014.

[59] Niels Bassler, Ioannis Kantemiris, Pantelis Karaiskos, Julia Engelke, Michael H. Holzscheiter, and Jørgen B. Petersen. Comparison of optimized single and multifield irradiation plans of antiproton, proton and carbon ion beams. *Radiotherapy and Oncology*, 95(1):87–93, April 2010.

[60] Leszek Grzanka. Cho cell depth-survival distributions after different configurations of contralateral carbon beams. In *3.rd ESTRO Forum*, 2015.

[61] Kristian Smeland Ytre-Hauge. Personal communication.

[62] M. Krämer, O. Jäkel, T. Haberer, G. Kraft, D. Schardt, and U. Weber. Treatment planning for heavy-ion radiotherapy: physical beam model and dose optimization. *Physics in Medicine and Biology*, 45(11):3299, November 2000.

[63] Thomas Haberer, Michael Kraemer, Gerhard Kraft, Wilma Kraft-Weyrather, Dieter Schardt, Michael Scholz, Ulrich Weber, Aleksiy Dolinski, Hartmut Eickhoff, Bernhard Franczak, and others. *Ion beam therapy system and a method for operating the system*. Google Patents, January 2004. US Patent 6,683,318.

[64] K. Parodi and W. Enghardt. Potential application of PET in quality assurance of proton therapy. *Physics in Medicine and Biology*, 45(11):N151, November 2000.

[65] Harald Paganetti. *Proton Therapy Physics*. Series in Medical Physics and Biomedical Engineering. CRC Press, Boca Raton, FL, 2012.

[66] Brita Singers Sørensen, Jens Overgaard, and Niels Bassler. In vitro RBE-LET dependence for multiple particle types. *Acta Oncologica*, 50(6):757–762, July 2011.

[67] International Commission on Radiological Protection. *ICRP Publication 60: 1990 Recommendations of the International Commission on Radiological Protection*. SAGE Publications, May 1991.

[68] P. Pihet, H. G. Menzel, R. Schmidt, M. Beauduin, and A. Wambersie. Biological Weighting Function for RBE Specification of Neutron Therapy Beams. Intercomparison of 9 European Centres. *Radiation Protection Dosimetry*, 31(1-4):437–442, June 1990.

[69] Harald Paganetti, Andrzej Niemierko, Marek Ancukiewicz, Leo E Gerweck, Michael Goitein, Jay S Loeffler, and Herman D Suit. Relative biological

effectiveness (RBE) values for proton beam therapy. *International Journal of Radiation Oncology*Biology*Physics*, 53(2):407–421, June 2002.

[70] Thomas Friedrich, Marco Durante, and Michael Scholz. Particle species dependence of cell survival RBE: Evident and not negligible. *Acta Oncologica*, 52(3):589–603, February 2013.

[71] M. Scholz. Effects of Ion Radiation on Cells and Tissues. In Henning Kausch, N. Anjum, Y. Chevolot, B. Gupta, D. Léonard, H. J. Mathieu, L. A. Pruitt, L. Ruiz-Taylor, and M. Scholz, editors, *Radiation Effects on Polymers for Biological Use*, number 162 in Advances in Polymer Science, pages 95–155. Springer Berlin Heidelberg, 2003.

[72] W. K. Weyrather, S. Ritter, M. Scholz, and G. Kraft. RBE for carbon track-segment irradiation in cell lines of differing repair capacity. *International Journal of Radiation Biology*, 75(11):1357–1364, November 1999.

[73] M. Scholz, W. Weyrather, M. Krämer, and Kraft. G. Modelling the increased biological effectiveness of heavy charged particles for tumour therapy treatment planning. In *Relative biological effectiveness in ion beam therapy, Report 461*. International Atomic Energy Agency, 2008.

[74] Michael C Joiner, Brian Marples, Philippe Lambin, Susan C Short, and Ingela Turesson. Low-dose hypersensitivity: current status and possible mechanisms. *International Journal of Radiation Oncology*Biology*Physics*, 49(2):379–389, February 2001.

[75] Minna Wedenberg and Iuliana Toma-Dasu. Disregarding RBE variation in treatment plan comparison may lead to bias in favor of proton plans. *Medical Physics*, 41(9):091706, September 2014.

[76] Clemens Grassberger, Alexei Trofimov, Anthony Lomax, and Harald Paganetti. Variations in linear energy transfer within clinical proton therapy fields and the potential for biological treatment planning. *International Journal of Radiation Oncology* Biology* Physics*, 80(5):1559–1566, 2011.

[77] J. Perl, J. Shin, J. Schumann, B. Faddegon, and H. Paganetti. TOPAS: an innovative proton Monte Carlo platform for research and clinical applications. *Medical Physics*, 39(11):6818–6837, November 2012.

[78] White paper 5 - Biology (web).pdf.

[79] Niels Bassler, Oliver Jäkel, Christian Skou Søndergaard, and Jørgen B. Petersen. Dose- and LET-painting with particle therapy. *Acta Oncologica*, 49(7):1170–1176, September 2010.

[80] Niels Bassler, Jakob Toftegaard, Armin Lühr, Brita Singers Sørensen, Emanuele Scifoni, Michael Krämer, Oliver Jäkel, Lise Saksø Mortensen, Jens Overgaard, and Jørgen B. Petersen. LET-painting increases tumour control probability in hypoxic tumours. *Acta Oncologica (Stockholm, Sweden)*, 53(1):25–32, January 2014.